

DEC 6 1956

UNCLASSIFIED

5

Copy

RM L56H01

NACA RM L56H01



RESEARCH MEMORANDUM

AERODYNAMIC AND HYDRODYNAMIC CHARACTERISTICS OF A
DECK-INLET MULTIJET WATER-BASED-AIRCRAFT CONFIGURATION
DESIGNED FOR SUPERSONIC FLIGHT

By Ralph P. Bielat, Claude W. Coffee, Jr.,
and William W. Petynia

CLASSIFICATION CHANGED

UNCLASSIFIED

Langley Aeronautical Laboratory
Langley Field, Va.

LIBRARY COPY

DEC 12 1956

LANGLEY AERONAUTICAL LABORATORY
LIBRARY NACA
LANGLEY FIELD, VIRGINIA

To _____
By authority of NACA TPA 11 *Effective* Date 12-1-59

JB 1-27-60

CLASSIFIED DOCUMENT

This material contains information affecting the national defense of the United States within the meaning of the espionage laws, Title 18, U.S.C., Sec. 793 and 794, the transmission or revelation of which in any manner to an unauthorized person is prohibited by law.

NATIONAL ADVISORY COMMITTEE FOR AERONAUTICS

WASHINGTON

December 5, 1956

~~CONFIDENTIAL~~

UNCLASSIFIED

NATIONAL ADVISORY COMMITTEE FOR AERONAUTICS

RESEARCH MEMORANDUM

AERODYNAMIC AND HYDRODYNAMIC CHARACTERISTICS OF A
DECK-INLET MULTIJET WATER-BASED-AIRCRAFT CONFIGURATION

DESIGNED FOR SUPERSONIC FLIGHT

By Ralph P. Bielat, Claude W. Coffee, Jr.,
and William W. Petynia

SUMMARY

The aerodynamic and hydrodynamic characteristics of a multijet water-based-aircraft configuration for supersonic operation have been investigated. The results of these tests have indicated that the model had a low subsonic drag and a relatively high Mach number for drag rise. The minimum drag coefficient for the basic configuration at a Mach number of 1.20 was 2.75 times the subsonic value. Pitch-up tendencies were indicated throughout the Mach number range at moderately high values of lift coefficient which would limit the operating ranges and performance characteristics of this configuration.

The time and distance for a stable take-off were approximately 34 seconds and 4,060 feet. An intermediate trim limit of stability in addition to upper and lower limits restricted the range of stabilizer and elevator deflections for stable take-offs. Porpoising occurred during all smooth-water landings but the oscillations damped rapidly. Brief rough-water tests indicate the inlets would be free from spray when operating in waves 4 feet high.

INTRODUCTION

The present investigation is part of a general research program to make a brief evaluation of the aerodynamic and hydrodynamic characteristics of a number of water-based bomber configurations capable of flight at transonic and supersonic speeds. The first two configurations in this program, a wing-root-inlet configuration and a nose-inlet configuration, were reported in references 1 and 2. These configurations had reduced water clearances from those of contemporary seaplanes, high-fineness-ratio hulls, and were designed in accordance with the transonic area-rule

~~CONFIDENTIAL~~
UNCLASSIFIED

concept (ref. 3). Aerodynamic tests over the Mach number range from 0.6 to 1.13 indicated low subsonic drag, high drag-rise Mach number, and low drag rise of these configurations. Hydrodynamic performance in smooth water was acceptable and inlets were clear of spray in moderate waves. In cooperation with the Bureau of Aeronautics and the aircraft industry, a third configuration was evolved which was designed for a Mach number of 1.35. In this configuration, an engine configuration which resulted in less internal ducting and more useful internal volume than the nose-inlet configuration and less frontal area than the wing-root-inlet configuration was achieved while maintaining adequate spray clearance. High fineness ratio and conformity with the supersonic area rule were maintained. (See refs. 4 and 5.)

In the present investigation, lift, drag, and pitching moment were determined over a Mach number range from 0.6 to 1.42. Smooth-water take-off and landing stability and resistance were investigated. A brief check of the rough-water spray and behavior was also made.

COEFFICIENTS AND SYMBOLS

Aerodynamic

The results of the wind-tunnel tests are referred to the wind-axes system. The aerodynamic moments are referred to the center of gravity of the model which is longitudinally located at 0.35 \bar{c} and is 8.7 feet full scale above the base line (fig. 1).

A	duct area
\bar{c}	mean aerodynamic chord of wing
C_D	drag coefficient, $\frac{D}{qS}$
C_{D_I}	internal-drag coefficient of ducts based on wing area
C_L	lift coefficient, $\frac{L}{qS}$
C_{L_α}	lift-curve slope, $\frac{dC_L}{d\alpha}$
C_m	pitching-moment coefficient, $\frac{M_{cg}}{qS\bar{c}}$

C_{mC_L}	pitching-moment-curve slope, $\frac{dC_m}{dC_L}$
C_p	pressure coefficient, $\frac{p_b - p_o}{q}$
D	drag
L	lift
L/D	lift-drag ratio
m	mass-flow rate, ρAV
M	Mach number
M_{cg}	pitching moment of aerodynamic forces about lateral axis which passes through center-of-gravity location
p	static pressure
q	free-stream dynamic pressure, $\frac{1}{2}\rho V^2$
R	Reynolds number based on \bar{c}
S	wing area
V	velocity
α	angle of attack referred to hull base line
ϵ	effective downwash angle
δ_e	elevator deflection referred to stabilizer chord, positive when trailing edge is down
δ_f	flap deflection, positive downward
δ_s	stabilizer incidence referred to hull base line, positive when trailing edge is down
ρ	air density
Subscripts:	
b	base

i duct inlet
o free stream
max maximum
min minimum

Hydrodynamic

A.P. after perpendicular
b hull beam
 C_{Δ_0} gross-load coefficient, $\frac{\Delta_0}{wb^3}$
F.P. forward perpendicular
 L_a afterbody length
 L_f forebody length
L.W.L. load water line
w specific weight of water, 63.3 lb/cu ft for these tests
 Δ_0 gross load
 τ trim, angle between forebody keel at step and the horizontal

DESCRIPTION OF CONFIGURATION

General arrangement drawings and hull layout are presented in figures 1 and 2, respectively. Pertinent dimensions and particulars are presented in table 1.

General Characteristics

Basic assumptions.- The gross weight of 200,000 pounds, wing area of 2,000 square feet, a bomb load of 30,000 pounds, and a rotating-type bomb bay were assumed. Four Curtiss-Wright J67 jet engines having a thrust of 88,000 pounds with afterburners were selected.

Engine location.- The jet engines were located in the hull (fig. 1). The inlets for the two forward engines were located on the side of the hull and the exhausts were below and slightly behind the wing trailing

edge. The afterburners were turned out from the center line approximately 8.5° . The inlet for the two aft engines was located on the hull deck aft of the juncture of the hull and wing trailing edge but ahead of the forward engine exhausts. These two engines were placed parallel to the center line and exhausted behind the vertical tail.

Wing.- The wing had an aspect ratio of 4.05, taper ratio of 0.333, 45° sweepback of the quarter-chord line, and embodied NACA 63A206 modified airfoil sections. The wing incidence at the root was 2° and the wing had a uniform twist of 5° .

Planing bottom.- The planing bottom extended the entire length of the airplane. The forebody length-beam ratio was 8.66 and the afterbody length-beam ratio was 7.44. The beam was set by the width of the bomb bay.

The forebody cross sections were rounded at the keel and approximated those proposed in references 6 and 7 for obtaining constant force during landing impacts. The step had a 64° vee plan form. Basically a deep step was used but a step fairing reduced the depth at the chine to 0.104 beam. The depth of step at the keel was 0.055 beam.

The angle of the afterbody keel and the height of the chine at the bow were kept low, so that the forebody and afterbody chines would follow as nearly as possible the stream flow lines.

Horizontal chine flare was used on the forebody from the bow to the step. The chine flare on the afterbody started approximately 18 feet aft of the point of the step and extended back to the after perpendicular. The forebody and afterbody dead rise was warped approximately 3° per beam in the vicinity of the step.

Tail group.- With the high beam loadings employed, a high horizontal-tail position was considered necessary for spray clearance.

Tip floats.- No tip floats were provided for this configuration as the wing is expected to provide the static transverse stability. The tip floats have been shown in reference 1 to contribute appreciably to the drag.

Area Curves

The total cross-sectional area curve for a Mach number of 1.35 and the contributions of the various components are presented in figure 3. The area distribution of the aerodynamic surfaces was taken as the cross-sectional area intersected by the Mach angle planes (for $M = 1.35$) rolled to 12 positions in intervals of 30° about the center line of the

~~CONFIDENTIAL~~

configuration. The cross-sectional areas obtained by the intersection of the Mach planes were averaged and this average area was then used for the body indentation. In order to simplify the calculations, the area distribution of the body was developed for a Mach number of 1.0 with the areas taken normal to the center line of the configuration. This procedure, as discussed in reference 5, would have a slight effect on the drag. An attempt was also made to distribute the hull cross-sectional area above and below the wing chord plane to minimize the drag due to lift. An equivalent free-stream tube area of 80 percent of the inlet area was subtracted for the mass flow through the ducts.

The maximum total cross-sectional area was approximately 147 square feet and the fineness ratio of the equivalent body was 11.8.

Wind-Tunnel Model

The wind-tunnel model employed for the aerodynamic tests was 1/52.7 size. Photographs of the model on the sting support in the Langley 8-foot transonic pressure tunnel are shown in figure 4. The model was constructed primarily of a skin made from plastic-impregnated fiber-glass cloth. The wing was made of aluminum and mahogany. The horizontal and vertical tail surfaces had steel cores which were welded together in order to add stiffness and to increase the load-carrying ability. Steel and mahogany were used in the hull to add stiffness and strength at critical points in the model. The aft end of the hull was cut off at approximately the exhaust of the rear engines in order to accommodate the sting support.

The model was unpowered but the jet-engine inlets were simulated. The rear inlet was raised off the deck approximately 1/16 inch (model scale) to provide for boundary-layer bypass. There was no boundary-layer bypass on the forward inlets. The ducting was designed to provide the proper mass flow. Constrictions in the area were placed in the duct exits for the purpose of evaluating the mass-flow and internal drag characteristics of the model.

The horizontal tail, which was of the all-movable type, was mounted on top of the vertical tail. The axis of rotation of the horizontal tail was taken about a lateral axis which passed through the quarter chord of the mean aerodynamic chord of the horizontal tail.

Some tests were conducted with fixed transition on the model by applying 1/8-inch-wide strips of no. 120 carborundum grains around the nose of the hull approximately 1 inch back from the nose, to the inlets at the leading edge of the inlets, and across the span of the wing at the 10-percent-chord station on both the upper and lower surfaces.

A modification to the basic hull indicated in figure 2 and in the area diagram of figure 3 was also investigated. The modification to the basic hull was intended to simulate the effects of a hot-jet exhaust that would be experienced on the full-scale configuration and gave a smoother area distribution in the region aft of the jet exhaust of the forward engines.

Tank Model

Photographs of the 1/17-size dynamic model are presented in figure 5. The hull of the model was of plastic impregnated fiber glass and the aerodynamic surfaces were of conventional wooden construction covered with silk.

Several modifications, which were principally extensions of the chine flare, were made to the tank model and were not incorporated on the wind-tunnel model as shown in figure 2. A chine strip, 0.7 foot (full size) deep at the step and faired into the chine approximately 34 feet (full size) forward of the step was added to the hull. This effectively extended the chine flare in the region of the step where the chine flare of the basic forebody was faded to zero. The sharp chines on the afterbody were extended forward to the step and a sharp chine was added to the fairing between the forward exhausts and the hull. These added chines would be expected to have a negligible effect on aerodynamics (ref. 1).

The wing used in the hydrodynamic tests was the same as that used with the nose-inlet configuration of reference 1. The differences in the wings used in the hydrodynamic and aerodynamic investigations were as follows: NACA 65A006 airfoil sections for the hydrodynamic wing instead of an NACA 63A206, aspect ratio of 4.0 instead of 4.05, a taper ratio of 0.3 instead of 0.333, and the wing was untwisted. The wing angle of incidence was $2\frac{1}{2}^{\circ}$. It is believed that the slight differences in the two wings would have a negligible effect upon the hydrodynamic tests. Leading-edge slots were used to prevent premature wing stall that usually is encountered at the low Reynolds numbers of tank tests. The full-span flaps were of the single slotted type and had fixed deflection angles of 0° and 40° .

The stabilizer deflection could be varied from 5° to -15° and the elevator deflection could be fixed at angles from 20° to -20° .

Electric contacts were located on the hull keel at the bow, step, and sternpost. These contacts indicated when these portions of the hull were in contact with the water and were also used to release the trim brake during the landing tests.

~~CONFIDENTIAL~~

APPARATUS AND PROCEDURES

Aerodynamic

Tunnel.- The aerodynamic investigations were conducted in the Langley 8-foot transonic pressure tunnel. The test section of this tunnel is rectangular in cross section. The upper and lower walls of the test section are slotted to permit continuous operation through the transonic speed range up to a Mach number of 1.20. The slots of the test section were removed and replaced with nozzle blocks to produce a Mach number of 1.42. The design of these nozzle blocks has been described in reference 8. For most of the aerodynamic investigation, the tunnel was operated at approximately one-half atmospheric stagnation pressure; however, a few of the tests were made at approximately atmospheric stagnation pressure. The dewpoint of the tunnel air was controlled and was kept between -10° F and 0° F. The stagnation temperature of the tunnel was automatically controlled and was kept constant and uniform across the tunnel at 124° F. Control of both dewpoint and stagnation temperatures in this manner minimized humidity effects.

Reynolds number.- The variation with Mach number of the range of Reynolds number based on the mean aerodynamic chord of the wing and a function of the stagnation pressure is shown in figure 6. For the present investigation, therefore, the Reynolds number varied from a minimum value of 0.73×10^6 at a Mach number of 0.60 to a maximum value of 1.89×10^6 at a Mach number of 1.20. The maximum Reynolds number at a Mach number of 1.42 was 1.86×10^6 .

Measurements.- Lift, drag, and pitching moment were determined by means of an electrical strain-gage balance located inside the hull. The measurements were taken over an angle-of-attack range from -4° to 14° for Mach numbers of 0.60 to 1.20 for the tests conducted at one-half atmospheric stagnation pressure. The angle-of-attack range was limited to approximately 6° for the tests made at atmospheric stagnation pressure because of strength limitations of the model. Static-pressure measurements were taken at two locations in the duct exits: one upstream and one downstream of the constriction in area, to determine the mass-flow and internal drag coefficient. No base-pressure adjustment for the nacelles was required because the nacelles were faired to a sharp edge. The base pressure at the aft end of the hull was also measured.

Corrections and accuracy.- No corrections to the free-stream Mach number and dynamic pressure for the effects of model and wake blockage are necessary for tests in the slotted test section of the Langley 8-foot transonic pressure tunnel (ref. 9). There is a range of Mach numbers above a Mach number of 1.00 where the data are affected by

~~CONFIDENTIAL~~

reflected compressions and expansions from the test-section boundary. From considerations of the results of reference 10, it is believed that for Mach numbers up to approximately 1.03, the effects of these disturbances on the measurements made in the present investigation would be negligible. No test data, however, were taken in the range ($M > 1.03$ and $M < 1.13$) where the reflected boundary disturbances impinged upon the model.

The drag data have been corrected for base pressure such that the base drag corresponds to conditions where the base pressure is equal to the free-stream static pressure. Typical variations of base pressure coefficient against angle of attack are given in figure 7. The internal drag has been also subtracted from the drag data to give a net external drag. The method for obtaining the internal drag is described in reference 1. The variation of the internal-drag coefficient with angle of attack is shown in figure 8. This drag coefficient is the total value of the four nacelles for the model.

No corrections for the forces and moments produced by the sting interference have been applied to the data. It is believed that the significant corrections would be limited to small increments in pitching moment and drag and to the effective downwash angle.

The angle of attack has been corrected for flow angularity and for the deflection of the sting-support system under load. The angle of attack is estimated to be accurate to within $\pm 0.1^\circ$.

The estimated consistency of the data at a Mach number of 0.90 and a stagnation pressure of 1,060 pounds per square foot, based on the static calibrations and the repeatability of the data, is as follows:

C_L	± 0.006
C_D	± 0.0008
C_m	± 0.006

Hydrodynamic

The hydrodynamic tests were made in Langley tank no. 1, which is described in reference 11. The apparatus and procedure generally used for testing dynamic models are described in reference 12 and were similar to those used for the investigation described in reference 1.

All tests were made at a gross load corresponding to 200,000 pounds, full size. The center of gravity was located at 0.358 unless otherwise noted. For the smooth-water investigation the model was pivoted at the center of gravity and had freedom in only trim and rise, and, for the

rough-water tests, the model also had fore and aft freedom. Slide wire pickups were used to record the trim and rise. Rise of the center of gravity was set zero with the step touching the water with the hull at zero trim. Trim was referenced to the forebody keel at the step and the undisturbed water surface.

The resistance of the complete model, including air drag, was determined for a range of constant speeds. No resistance data were obtained when the model was porpoising. A flap deflection of 0° was used up to a speed of approximately 100 knots (full size) and full flap deflection, 40° , was used at the higher speeds. The air drag of the towing staff was subtracted as a tare from the total resistance. Spray observations and photographs were obtained during these runs.

The trim limits of stability were determined during constant speed runs. At each speed, the trim of the hull was changed by adjusting the stabilizer position until porpoising was noted or until the maximum or minimum stabilizer deflection was obtained. The trim at which porpoising was first observed was taken as the limit of stability. The lower trim limit of stability was obtained with the center of gravity moved forward to 0.25 \bar{c} .

The rate of acceleration of 5 ft/sec² for take-off was based on an average value of excess thrust as determined from the constant speed resistance tests. A flap deflection of 0° was used until a speed of 80 knots and a flap deflection of 40° was used from 80 knots to take-off. Observation and motion pictures were made during these runs.

Landings were made with full down flaps for a range of contact trims. With the model flying at the desired landing trim, the carriage was decelerated at various uniform rates allowing the model to glide onto the water. The model was held at the desired landing trim by the trim brake until contact with the water surface.

RESULTS AND DISCUSSION

Aerodynamic

The basic aerodynamic data for the model are presented in figures 9 to 12. The variation of mass-flow ratio with angle of attack for the Mach number range of 0.60 to 1.42 is given in figure 13. It will be noted that the experimentally measured values of mass-flow ratio for the forward inlets and the rear deck inlet approximate the design mass-flow ratio of 0.80.

~~CONFIDENTIAL~~

Drag characteristics.- A comparison of the minimum drag coefficients for the basic configuration and for the modified configuration is presented in figure 14. The minimum subsonic drag coefficient for both configurations was approximately 0.0145. The drag-rise Mach number (defined as the value where $\frac{dC_D}{dM} = 0.1$) was about 0.93 for the basic configuration and approximately 0.95 for the modified configuration. The minimum drag coefficient for the basic configuration at a Mach number of 1.20 increased the subsonic value by a factor of 2.75. The modification made to the hull (simulating the jet exhaust area) resulted in about a 5 percent reduction in the minimum drag at a Mach number of 1.20 as compared with the basic configuration. The effect of the modification on the internal drag of the forward engines is not known since internal-flow measurements with the modified configuration were not made. It will be noted that the minimum drag coefficient for both the basic and modified configurations continues to increase in the supersonic range.

Some of the tests for the basic configuration were repeated with fixed transition on various parts of the model. Although the absolute values of the drag coefficient were higher for the configuration with fixed transition (fig. 11), it will be noted that the transonic drag-rise increment is approximately 13 percent lower for the basic model with fixed transition as compared with the basic model with natural transition.

An increase in the Reynolds numbers of the tests had no effect on the drag characteristics of the modified configuration as shown in figure 12.

The data presented in figure 9 have been used to calculate the trimmed lift-drag ratios for the basic model which are shown in figure 15. Some of the data shown in figure 15 were extrapolated and interpolated because only a small range of stabilizer incidence settings was used. It will be noted that the trimmed $(L/D)_{max}$ decreased quite rapidly for Mach numbers above 0.90. It will also be noted that the lift coefficient for trimmed $(L/D)_{max}$ increased from a value of 0.30 at a Mach number of 0.60 to approximately 0.40 at a Mach number of 1.20.

The variation of trimmed $(L/D)_{max}$ against Mach number for the basic configuration is given in figure 16. The trimmed $(L/D)_{max}$ decreased from a value of 13.3 at $M = 0.60$ to 6.0 at $M = 1.20$. The values of trimmed lift-drag ratio for level flight at sea level and an altitude of 35,000 feet for a wing loading of 100 pounds per square foot are also shown in figure 16. In order to take advantage of the high value of L/D at a Mach number of 0.90, for example, an altitude of approximately 35,000 feet would be required; however, the maneuverability would be limited since the lift coefficient for trimmed $(L/D)_{max}$ is

~~CONFIDENTIAL~~

slightly below the lift coefficient for the unstable break in pitching moment.

The modification to the hull caused some small increases in the untrimmed $(L/D)_{\max}$ at Mach number greater than 0.95 (fig. 17) when compared with the basic model.

Lift characteristics.— Both the basic configuration and the modified configuration exhibited nonlinear lift characteristics in the angle range of -4° to 0° . (See figs. 9 and 10.) However, when transition was fixed on the basic model (fig. 11) or when the Reynolds numbers of the tests of the modified configuration were increased by increasing the stagnation pressure (fig. 12), the lift characteristics were linear over an angle range of -4° to 6° .

The lift-curve slopes for various model configurations and test conditions have been determined and are presented in figure 18. In general, the lift-curve slopes increased to a maximum value at Mach number of about 0.95 and then decreased gradually with increase in speed. The lift-curve slope of the basic configuration for the trimmed condition (fig. 18(a)) was approximately $5\frac{1}{2}$ percent lower than for the untrimmed condition at a Mach number of 0.60 and 10 percent lower at a Mach number of 1.20. The decrease in lift-curve slope noted for the modified configuration for Mach numbers of 0.90 and above (fig. 18(c)) for the tests conducted at a stagnation pressure of 2,120 pounds per square foot is believed to be due to an increase in wing twist for the higher density loads rather than due to scale effects.

Pitching-moment characteristics.— The pitching-moment characteristics for the basic configuration without the horizontal tail (fig. 9) indicated pitch-up tendencies at lift coefficients approximately 0.2 to 0.6 throughout the Mach number range. The addition of the high horizontal tail aggravated the pitch-up instability; however, the lift coefficient at which the unstable break occurred was delayed to much higher values. Similar pitch-up characteristics have been observed for other model configurations having moderately high horizontal-tail arrangements. (See ref. 13, for instance.) The maximum operating range of altitudes of this configuration would be restricted because of the pitch-up tendencies which, for example, would be limited to approximately 46,000 feet at a Mach number of 0.90.

Fixing transition on the basic model made the pitching moments slightly more negative (fig. 11); however, the pitching-moment characteristics were essentially the same as for the basic model with natural transition.

The pitching-moment-curve slopes C_{mC_L} averaged over a lift-coefficient range of -0.1 to 0.1 for the basic model with the horizontal tail off and measured at $C_m = 0$ for several complete model configurations have been determined and are presented in figure 19. The usual rearward movement of the aerodynamic-center location with increase in Mach number for the basic configuration with the horizontal tail on and off is indicated (fig. 19(a)). Figure 19(b) compares the pitching-moment-curve slopes for the basic and the modified configurations and, in general, the pitching-moment-curve slopes were nearly the same for both configurations. Increasing the Reynolds numbers of the tests by increasing the stagnation pressure made the modified configuration less stable through the lift range (fig. 12) and Mach number range (fig. 19(c)). It is believed that part of the reduction in stability for the higher Reynolds numbers was due to an increase of wing twist for the higher density loads.

Stabilizer effectiveness.— The stabilizer-effectiveness parameter for the basic configuration averaged over a lift-coefficient range of 0 to 0.6 is presented in figure 20. The stabilizer effectiveness gradually increased to a value of -0.0265 at a Mach number of 0.90 and then decreased approximately 17 percent through the transonic-speed range.

Effective downwash characteristics.— The variation of the effective downwash angle with angle of attack for the basic configuration is shown in figure 21. The effective downwash angle at a given angle of attack was determined by finding the stabilizer incidence setting at which the pitching-moment coefficient of the complete configuration was equal to that of the complete configuration less the horizontal tail. (See fig. 9.) The effect of the horizontal-tail drag on the pitching moment was neglected. Since only a small range of stabilizer incidence settings was used, some of the data at the low and at the high angles of attack given in figure 21 were extrapolated. The effective downwash angles so determined do not entirely represent the flow angularities that exist in the region of the horizontal tail but also include various interference effects. The effective downwash angle increased quite markedly at angles of attack above about 6° throughout the Mach number range. These large increases in the effective downwash angle at high angles of attack reflect the severity of the pitch-up characteristics that were noted for the complete model. It should also be noted that large increases in the absolute values of the effective downwash angle occurred near 0° angle of attack at Mach numbers of 1.15 and 1.20.

The downwash derivative $\partial\epsilon/\partial\alpha$ for the basic configuration averaged over the angle-of-attack range of -2° to 2° and 10° to 12° is given in figure 22. The downwash derivative for the angle-of-attack range of -2° to 2° remained fairly constant up to a Mach number of 0.95 and then decreased to a value of zero at a Mach number of 1.20. In the

angle-of-attack range of 10° to 12° , the value of the downwash derivative was approximately four times that obtained at angles of attack of -2° to 2° for subsonic Mach numbers and had a value greater than 1.0 for Mach numbers of 0.70 to 0.98. The increase in the derivative $\partial \epsilon / \partial \alpha$ emphasizes the marked increase in the pitch-up tendencies at high angles of attack for the basic model with horizontal tail.

Hydrodynamic

During the initial hydrodynamic tests of the model, a yawing tendency was observed. The yawing appeared to be caused by spray from the step flowing over the rounded sections of the afterbody. The addition of the sharp chines on the afterbody and chine strips on the forebody improved the flow about the model and alleviated the yawing tendency.

Typical spray photographs in smooth water are presented in figure 23. No spray entered the side or deck inlets at any speed. No air flow through the jet inlets was simulated but unpublished tank data indicated that the simulation of the air flow would have little effect upon the spray pattern in the proximity of the inlets. Less is known about the effect of the exhausts on the water flow about the model. The under-surface of the wing was heavily wetted by bow spray from 40 to 86 knots. When the flaps were deflected, they were heavily wetted up to a speed of 105 knots. From 86 knots to take-off speed, the horizontal tail was struck by heavy spray that appeared to originate on the step aft of the forebody chine strips. The portions of the ducts for the rear engines which extended outboard of the afterbody chine were wetted by spray throughout most of the speed range.

The total resistance and corresponding trim and rise are presented in figure 24 for 0° and 40° flaps and several stabilizer and elevator positions. The stabilizer and elevators had little effect on the trim from hump speed to approximately 110 knots. The lack of trim control in this speed range appears to be caused by the low sternpost angle (6.4°) and the long afterbody running in the wake from the forebody. At approximately 105 knots, the resistance increased with little change in trim. This increase in resistance at high speeds has been encountered with configurations of reference 1 and occurs when the forebody flow reattaches to the afterbody due to insufficient clearance from the forebody wake at moderately high trims. At higher speed, the trim began to decrease (approximately 110 knots), reducing the flow on the afterbody, with a consequent reduction in resistance as may be noted at approximately 120 knots with a stabilizer and elevator setting of -10° and -20° , respectively. At a speed of 98 knots (fig. 24) it may be noted that deflection of the flaps to 40° resulted in a rise of about 0.5 foot due to the increased lift with the flaps deflected. No corresponding decrease in resistance is noted, however, apparently because of the heavy spray

striking the deflected flap. Full deflection of the flaps is therefore of little advantage until high speeds are reached. Excess thrust was available for acceleration throughout the speed range. A stable take-off can be made in approximately $\frac{3}{4}$ seconds and 4,060 feet.

The trim limits of stability are presented in figure 25. An instability at intermediate trims between the conventional upper and lower trim limits was encountered with this model. This intermediate porpoising was similar to that obtained in other tank tests (unpublished data). This intermediate limit was difficult to define because of a tendency of the model to maintain a constant trim in this speed region in spite of the application of a fairly large nose-down moment by deflection of the elevator and stabilizer. However, once the model did begin to change trim, it trimmed down quite rapidly. Since the intermediate trim limit was apparently encountered during this rapid trim change, it was difficult to determine at what trim instability first occurred. Once the instability at the intermediate trims was encountered, porpoising between the intermediate and upper trim limits usually resulted.

Typical variations in trim and rise during take-offs are presented in figure 26 for three stabilizer and elevator deflections. A flap deflection of 0° was used to approximately 80 knots and full flap deflection (40°) from 80 knots to take-off. The trims were high but tended to be slightly lower than the upper-trim limit up to a speed of approximately 115 knots. At this speed the flow from the forebody apparently broke away from the afterbody and the model trimmed down rapidly except at the maximum up stabilizer (-15°) and elevator (-20°) deflection. At the maximum up stabilizer and elevator deflection there was a slight decrease in trim before the model trimmed into the upper-trim limit. With a stabilizer deflection of -10° and an elevator deflection of -20° , the model trimmed between the intermediate and upper-trim limits and a stable take-off was made. When a stabilizer deflection of -8.5° and an elevator deflection of -17° were used, the model trimmed down rapidly into the intermediate-trim limit and porpoised between the intermediate and upper-trim limits.

The variations in trim and rise during typical landing at 6° and 12° trim are presented in figure 27. Porpoising occurred during all landings. The maximum amplitude of porpoising was approximately 5° but damped rapidly. This porpoising was caused either by landing at trims that were above the upper-trim limit of stability or by the trimming of the model into the intermediate limit during the landing runout. At landing trims below the upper limit, the model trimmed into the intermediate limit and porpoised between the intermediate and the upper-trim limits of stability.

Rough Water

A brief rough-water investigation was made with landings and taxiing in waves of various heights and lengths to determine the extent of spray entering the inlets and the amplitudes of the model motions in trim and rise. Oscillograph records of the variations in trim and rise during two typical landings at a trim of 9.2° in waves 4 and 8 feet high and 255 feet long are shown in figure 28. Comparison of these records shows that the motions were not violent when landing in waves 4 feet high. The maximum amplitudes of trim and rise were 8° and 12 feet and no spray entered the inlets when taxiing or landing in waves of this height. By contrast, the records indicate the large amplitudes of trim and rise (maximum for the landing shown 21.3° and 31.1 feet) when landing in the 8-foot waves. Heavy spray passed over the bow and entered the forward inlets during the violent landing motions in this wave height.

CONCLUDING REMARKS

The aerodynamic and hydrodynamic characteristics of a multijet water-based-aircraft configuration for supersonic flight have been investigated. The results of these tests have indicated that the basic configuration had a low subsonic drag and the drag rise delayed to a relatively high Mach number. The minimum drag coefficient at a Mach number of 1.20 was 2.75 times the minimum subsonic value. Pitch-up tendencies were indicated throughout the Mach number range at moderately high values of lift coefficient which would limit the operating ranges and performance characteristics of this configuration.

The time and distance for a stable take-off were approximately 34 seconds and 4,060 feet. An intermediate-trim limit of stability in addition to upper and lower limits restricted the range of stabilizer and elevator deflections for stable take-offs. Porpoising occurred during all smooth-water landings but the oscillations damped rapidly. Brief rough-water tests indicate the inlets would be free from spray when operating in waves 4 feet high.

Langley Aeronautical Laboratory,
National Advisory Committee for Aeronautics,
Langley Field, Va., July 27, 1956.

REFERENCES

1. Olson, Roland E., and Bielat, Ralph P.: An Aerodynamic and Hydrodynamic Investigation of Two Multijet Water-Based Aircraft Having Low Transonic Drag Rise. NACA RM L55A11a, 1955.
2. McKann, Robert E., and Coffee, Claude W.: Limited Hydrodynamic Investigation of a 1/15-Size Model of a Modified Nose-Inlet Multijet Water-Based Aircraft. NACA RM L55J19, 1956.
3. Whitcomb, Richard T.: A Study of the Zero-Lift Drag-Rise Characteristics of Wing-Body Combinations Near the Speed of Sound. NACA RM L52H08, 1952.
4. Whitcomb, Richard T., and Fischetti, Thomas L.: Development of a Supersonic Area Rule and an Application to the Design of a Wing-Body Combination Having High Lift-to-Drag Ratios. NACA RM L53H31a, 1953.
5. Whitcomb, Richard T.: Some Considerations Regarding the Application of the Supersonic Area Rule to the Design of Airplane Fuselages. NACA RM L56E23a, 1956.
6. Wagner, Herbert: Landing of Seaplanes. NACA TM 622, 1931.
7. Bisplinghoff, R. L., and Doherty, C. S.: A Two-Dimensional Study of the Impact of Wedges on a Water Surface. Contract No. NOa(s)-9921, Dept. Aero. Eng., M.I.T., Mar. 20, 1950.
8. Matthews, Clarence W.: An Investigation of the Adaptation of a Transonic Slotted Tunnel to Supersonic Operation by Enclosing the Slots With Fairings. NACA RM L55H15, 1955.
9. Wright, Ray H., and Ward, Vernon G.: NACA Transonic Wind-Tunnel Test Sections. NACA Rep. 1231, 1955. (Supersedes NACA RM L8J06.)
10. Ritchie, Virgil S., and Pearson, Albin O.: Calibration of the Slotted Test Section of the Langley 8-Foot Transonic Tunnel and Preliminary Experimental Investigation of Boundary-Reflected Disturbances. NACA RM L51K14, 1952.
11. Truscott, Starr: The Enlarged N.A.C.A. Tank, and Some of Its Work. NACA TM 918, 1939.

12. Olson, Roland E., and Land, Norman S.: Methods Used in the NACA Tank for the Investigation of the Longitudinal-Stability Characteristics of Models of Flying Boats. NACA Rep. 753, 1943.
(Supersedes NACA WR L-409.)
13. Weil, Joseph, and Gray, W. H.: Recent Design Studies Directed Toward Elimination of Pitch-Up. NACA RM L53I23c, 1953.

TABLE I.- PERTINENT CHARACTERISTICS AND DIMENSIONS OF THE
FULL-SIZE WATER-BASED AIRCRAFT

General:		
Gross weight, lb		200,000
Wing area, sq ft		2,000
Engines, Curtiss-Wright J67		4
Take-off thrust (with afterburners), lb		88,000
Wing loading, lb/sq ft		100
Take-off thrust-weight ratio		0.44
Wing:		
Span, ft		30.0
Airfoil section	NACA 63A206	Mod.
Aspect ratio		4.05
Taper ratio		0.333
Sweepback (0.25 \bar{c}), deg		45
Dihedral, deg		-1.47
Length, mean aerodynamic chord, ft		23.9
Forward perpendicular to L.E. of M.A.C., ft		69.0
Incidence, deg		
Root		2
Tip		-3
Horizontal tail:		
Span, ft		32.5
Airfoil section	NACA 63A006	
Area, sq ft		314
Aspect ratio		3.36
Taper ratio		0.5
Sweepback (0.25 \bar{c}), deg		45
Dihedral, deg		15
Arm, between quarter-chords, ft		74.8
Vertical tail:		
Airfoil section	NACA 63A008	
Aspect ratio		1.0
Sweepback (0.25 \bar{c}), deg		50
Bullet fairing	NACA 64-1A012	
Hull:		
Forebody length (forward perpendicular to step centroid), ft		79.40
Afterbody length (step centroid to after perpendicular), ft		68.25
Length, overall, ft		147.65
Beam at chines, maximum, ft		9.17
Width, maximum, ft		9.33
Height, maximum, ft		15.67
Step plan form	64° Vee	
Step depth at keel, ft		0.5
Step depth at chine, ft		0.96
Deadrise at step, basic, deg		30
Deadrise at after perpendicular, deg		54.5
Afterbody keel angle, deg		6
Steepness angle, deg		6.4
Center of gravity, 0.35 \bar{c}		
Above base line, ft		8.7
Forward of step centroid, ft		2.03
Step centroid to 0.35 \bar{c} , angle to vertical, deg		13.05
Hull volume, cu ft		11,805
Ratio of hull excess buoyancy to gross load		2.78
$\frac{I_x}{b_{max}}$		8.66
$\frac{I_y}{b_{max}}$		7.44
$\frac{(I_x + I_y)}{b_{max}}$		16.11
$C_{\Delta 0}$		4.06
Area curves:		
Maximum net cross-sectional area, sq ft		147
Maximum diameter of equivalent body, ft		13.9
Length, ft		163.0
Fineness ratio of equivalent body		11.8
Ratio of maximum hull cross-sectional area to wing area		0.064
Total surface area, sq ft		9,212

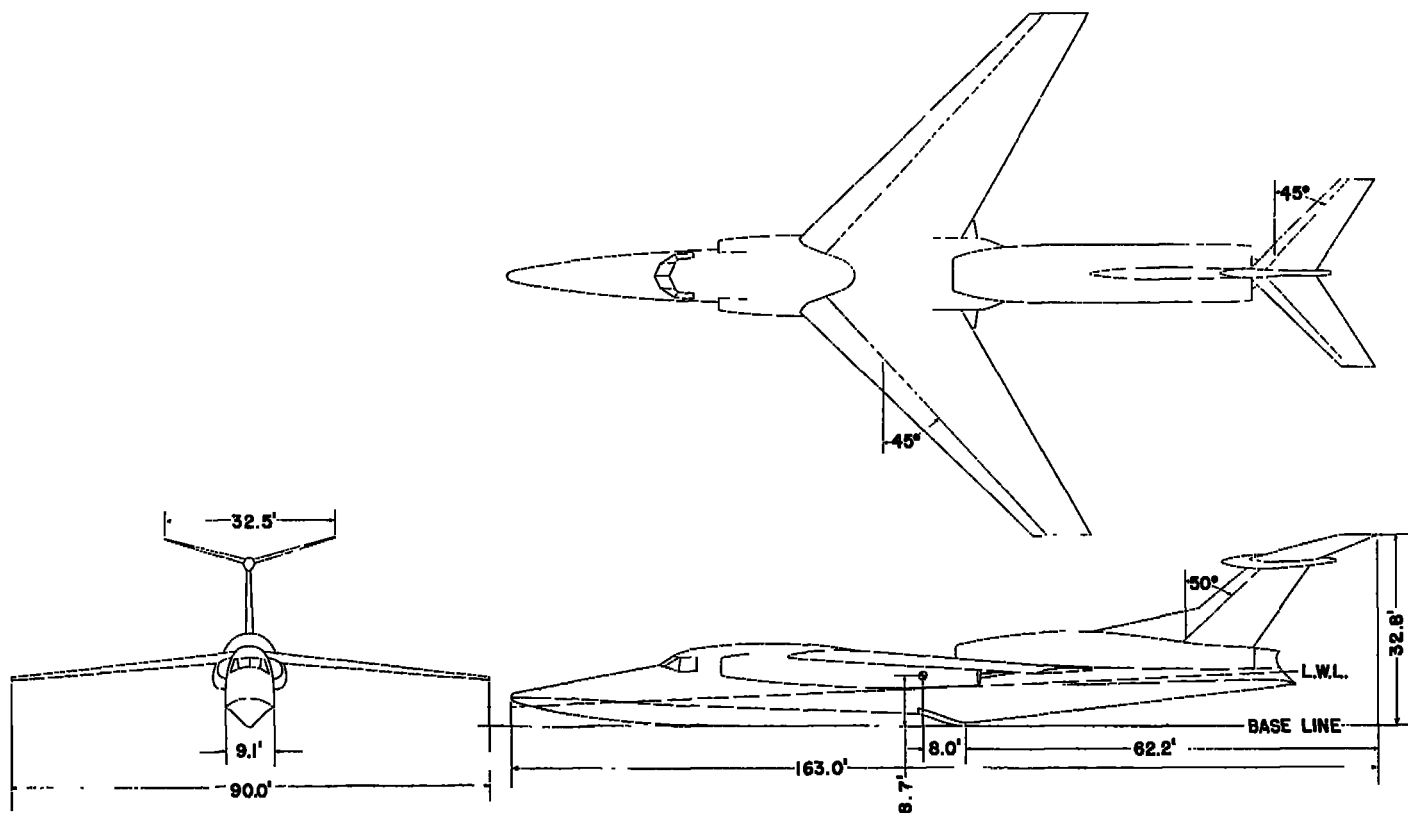


Figure 1.- General arrangement of deck-inlet configuration.

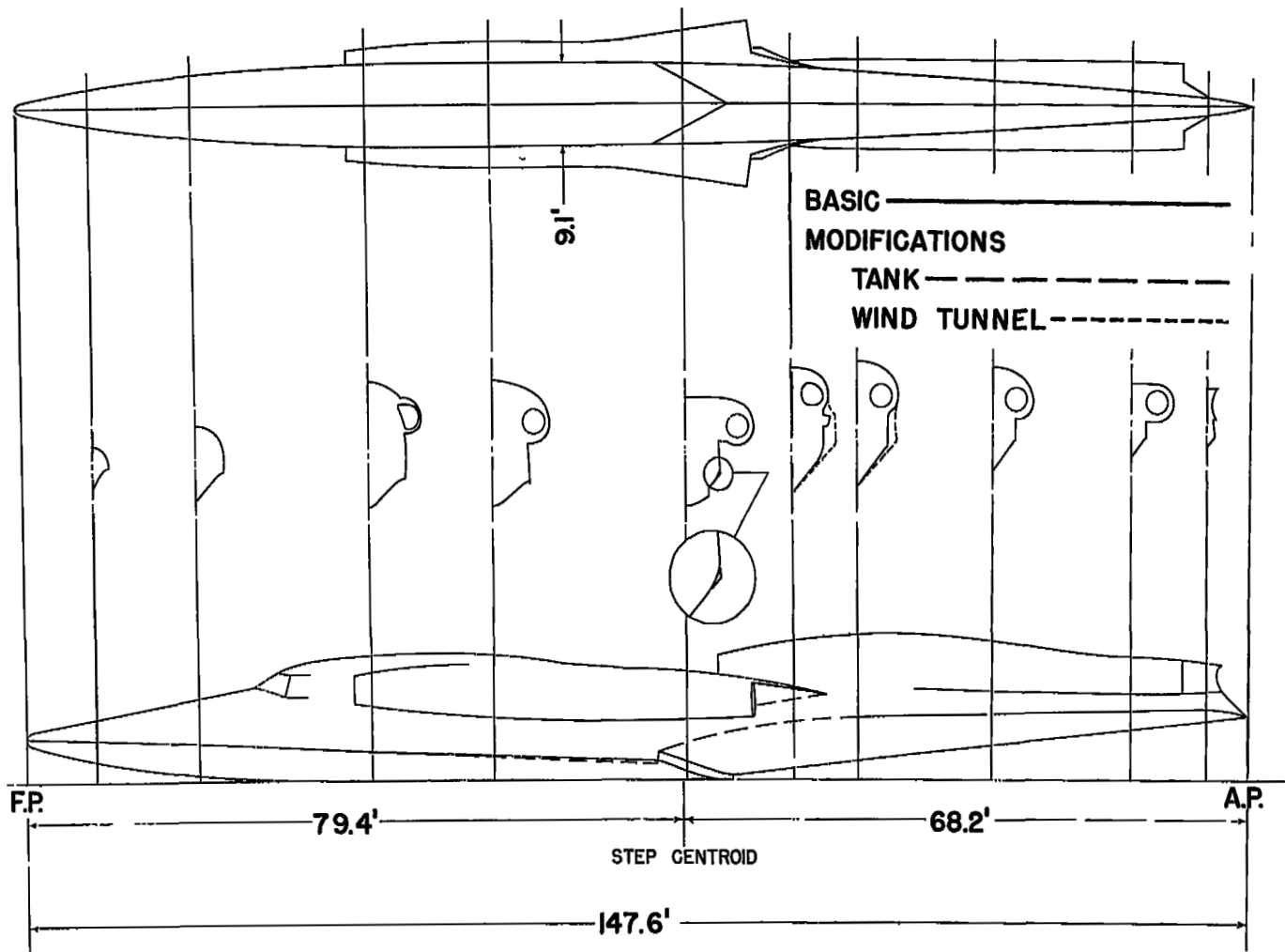


Figure 2.- Layout of deck-inlet configuration hull.

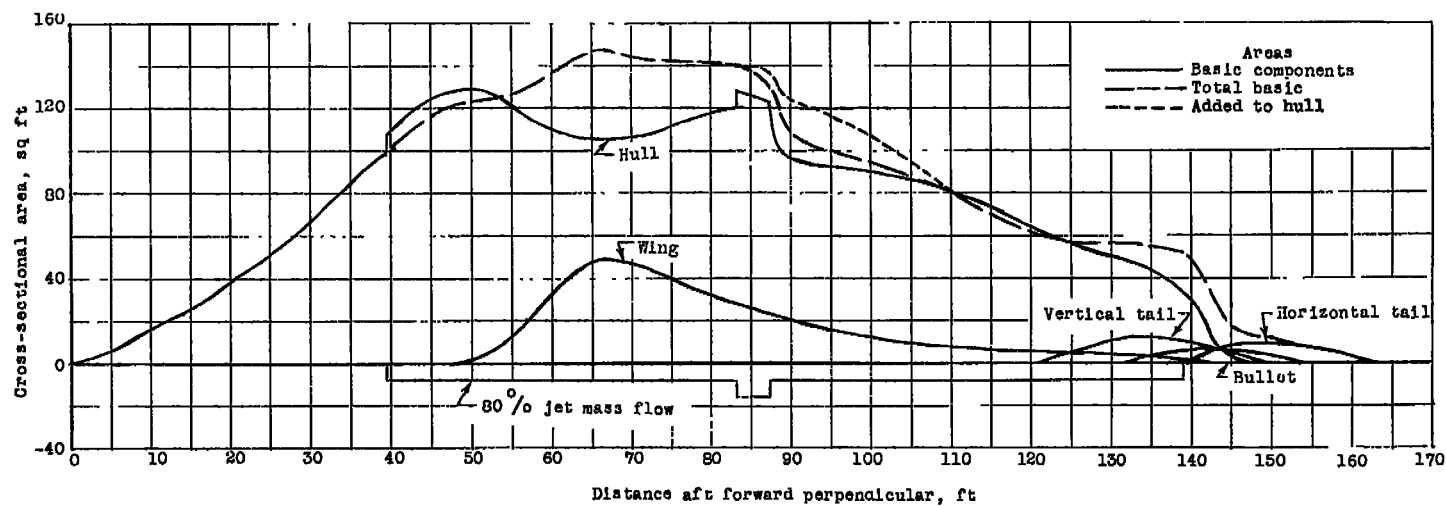
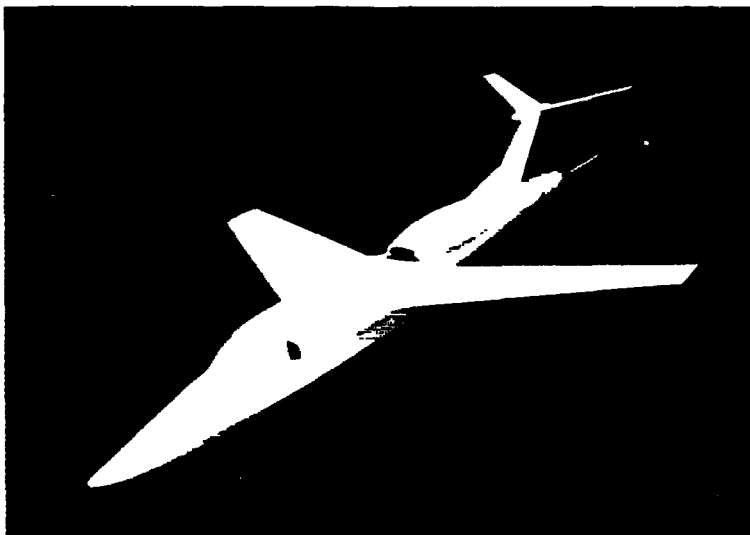
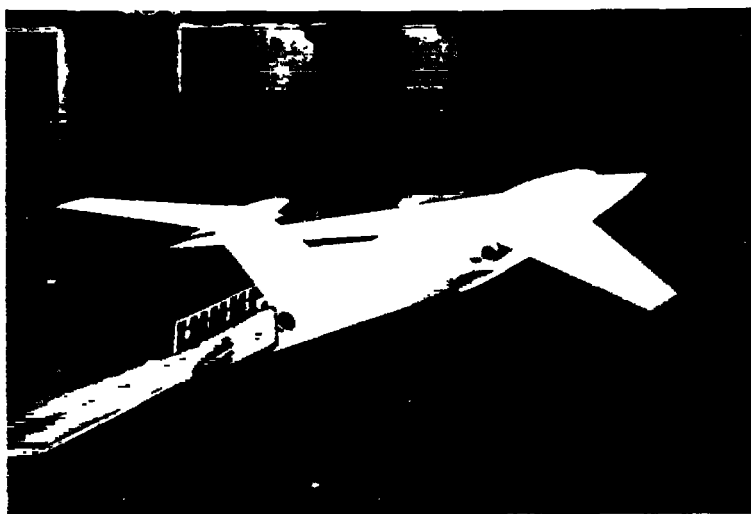


Figure 3.- Cross-sectional area curves. $M = 1.35$.



(a) Three-quarter front view.

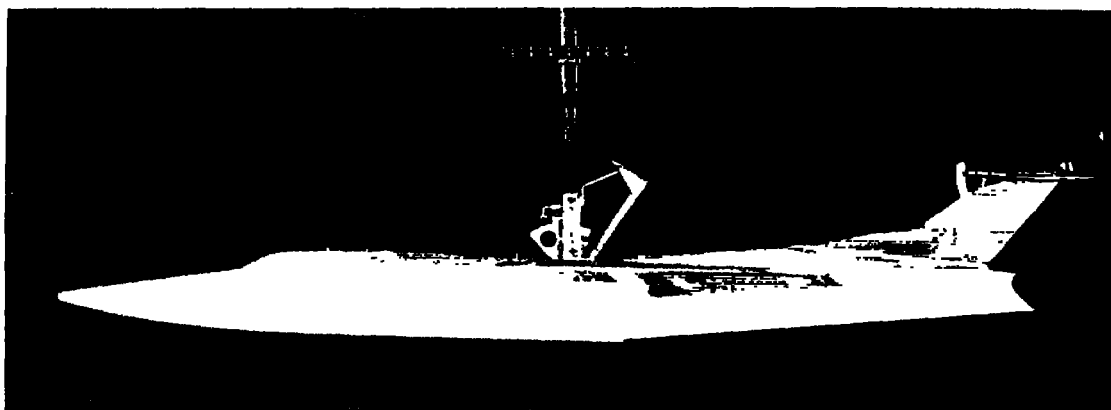
L-91010



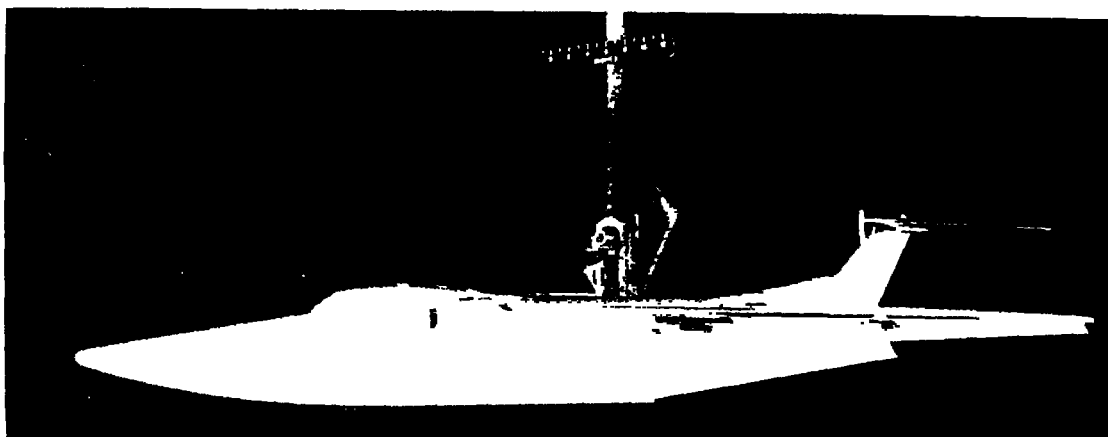
(b) Three-quarter rear view.

L-91009

Figure 4.- The $1/52.7$ -size wind-tunnel model on sting support in Langley 8-foot transonic pressure tunnel.



L-89710



L-89709

Figure 5.- The 1/17-size model of deck-inlet aircraft.

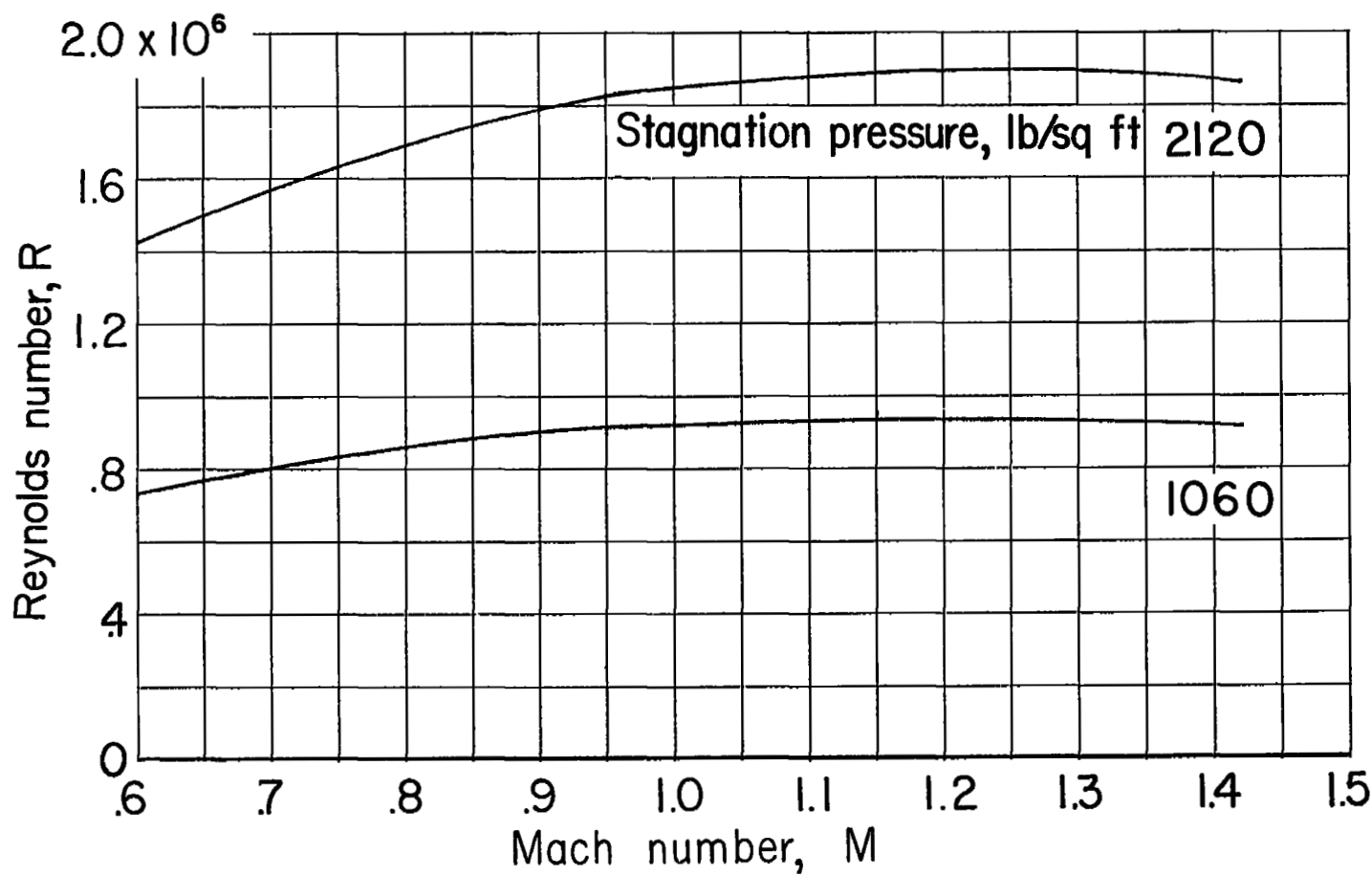


Figure 6.- Variation with Mach number of the test Reynolds number range based on wing mean aerodynamic chord.

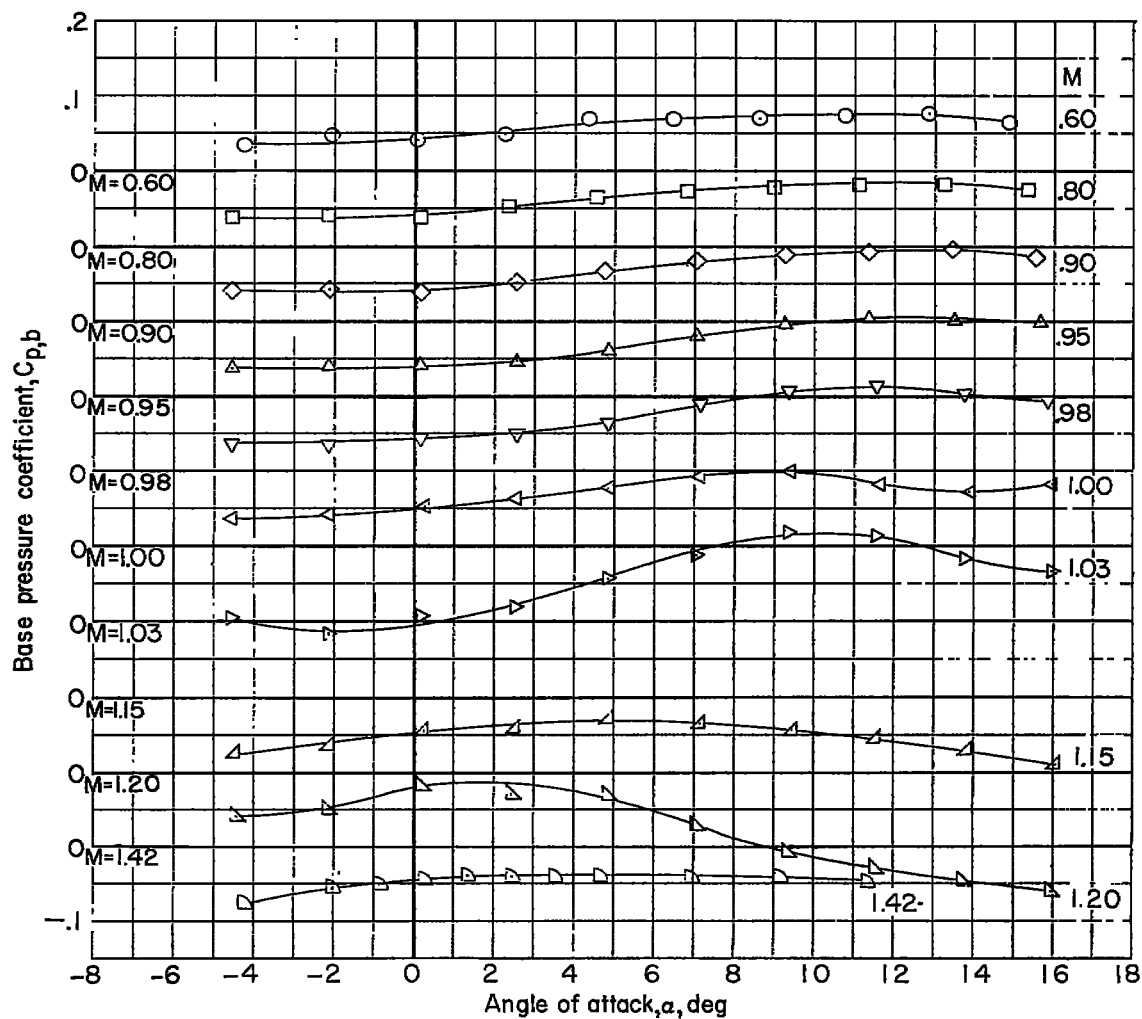


Figure 7.- Variation with angle of attack of base pressure coefficient for the basic configuration.

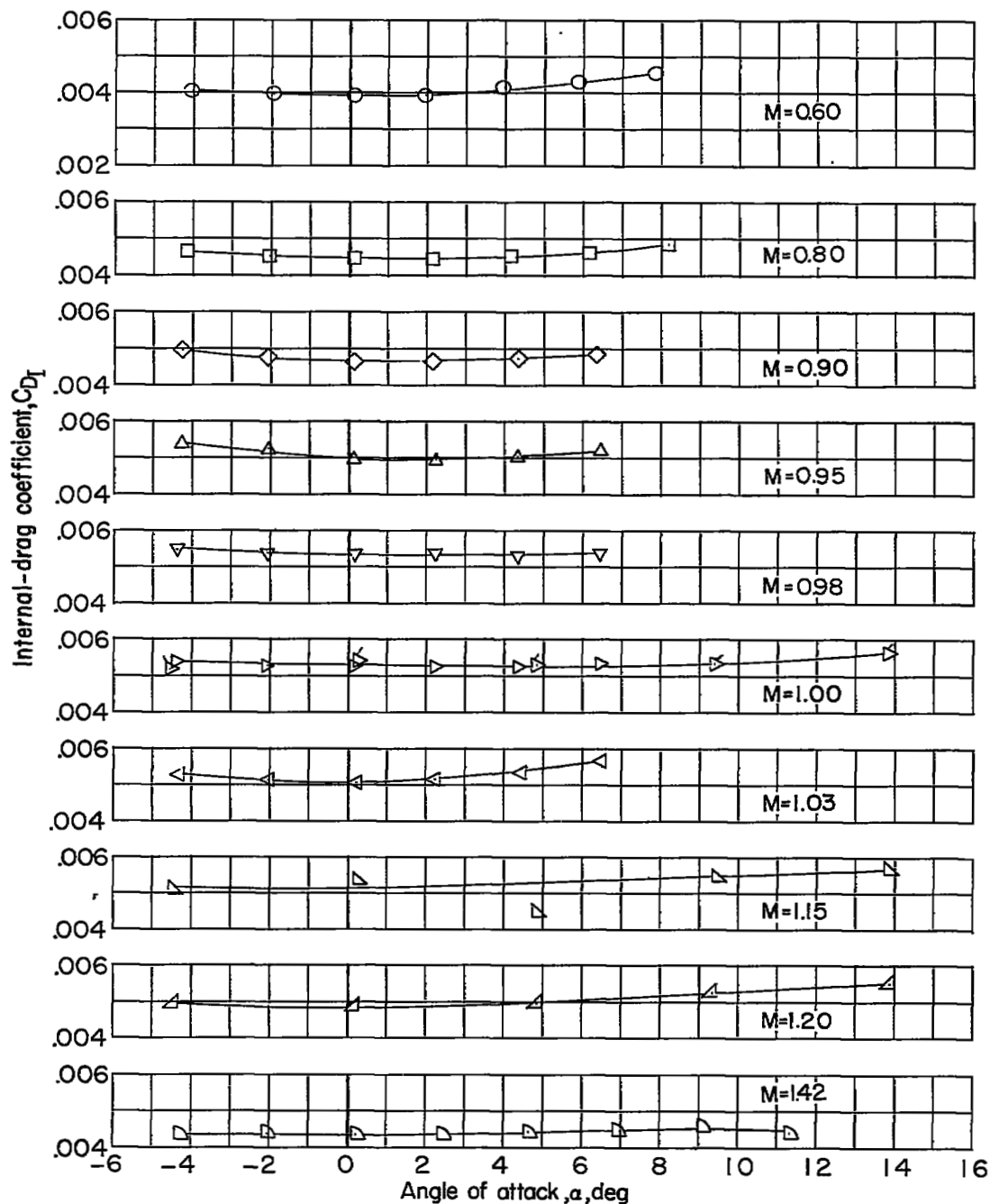


Figure 8.- Variation with angle of attack of the internal-drag coefficient for the basic configuration. Flagged symbols indicate repeat data.

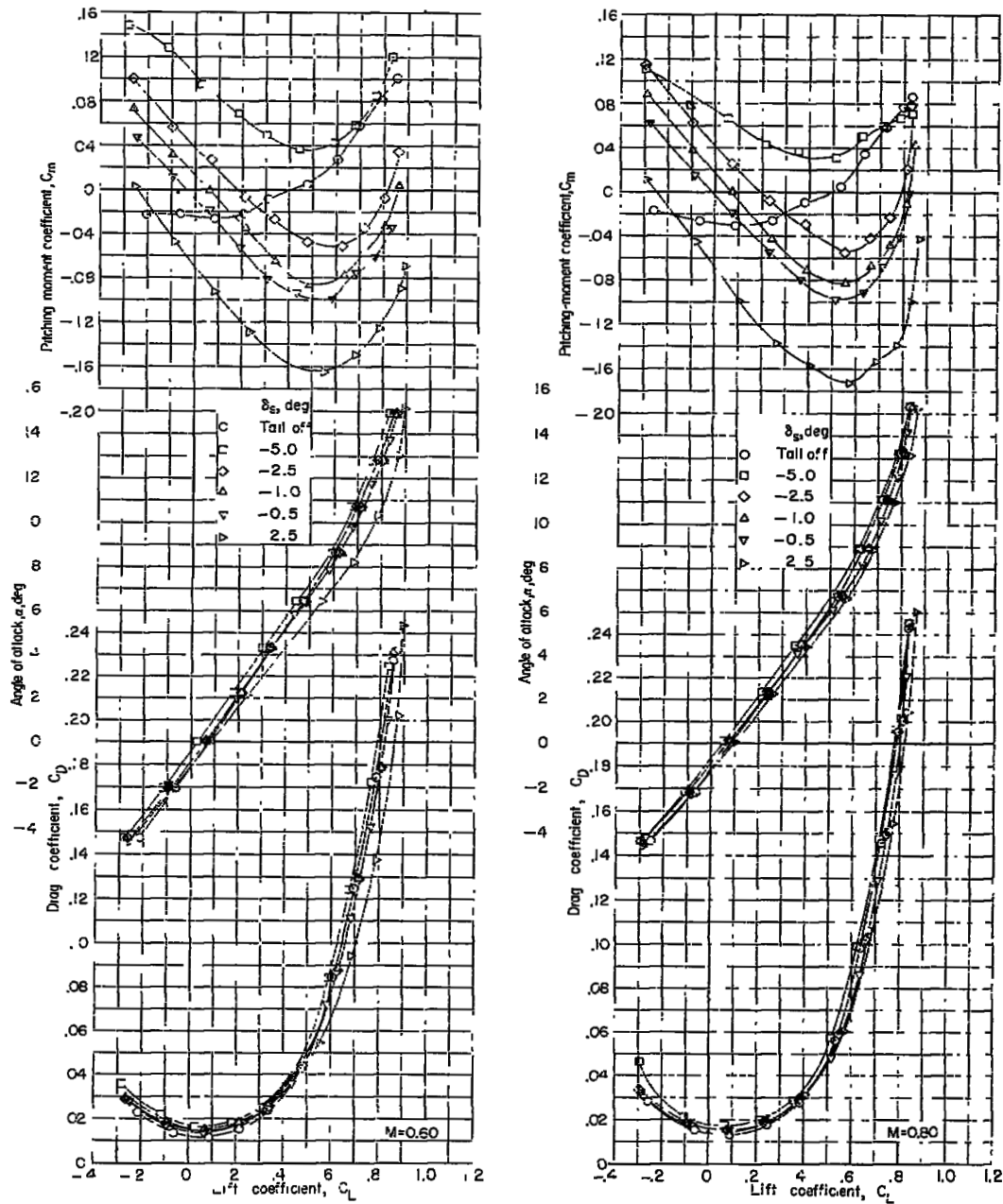
(a) $M = 0.60$ and 0.80 .

Figure 9.- Effect of stabilizer incidence on the aerodynamic characteristics of the basic model.

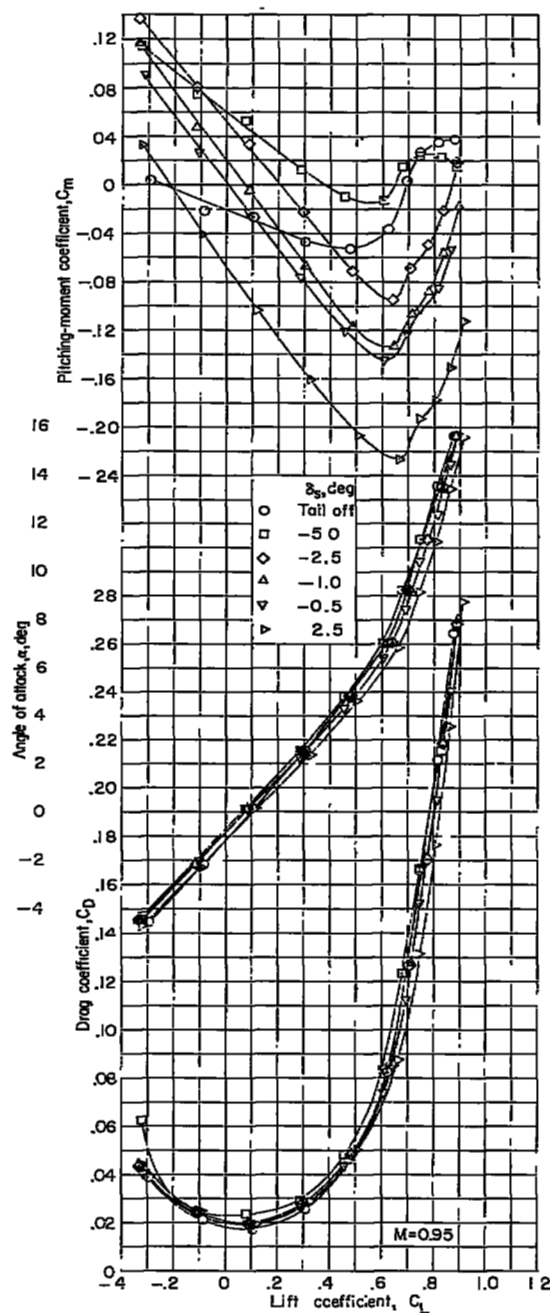
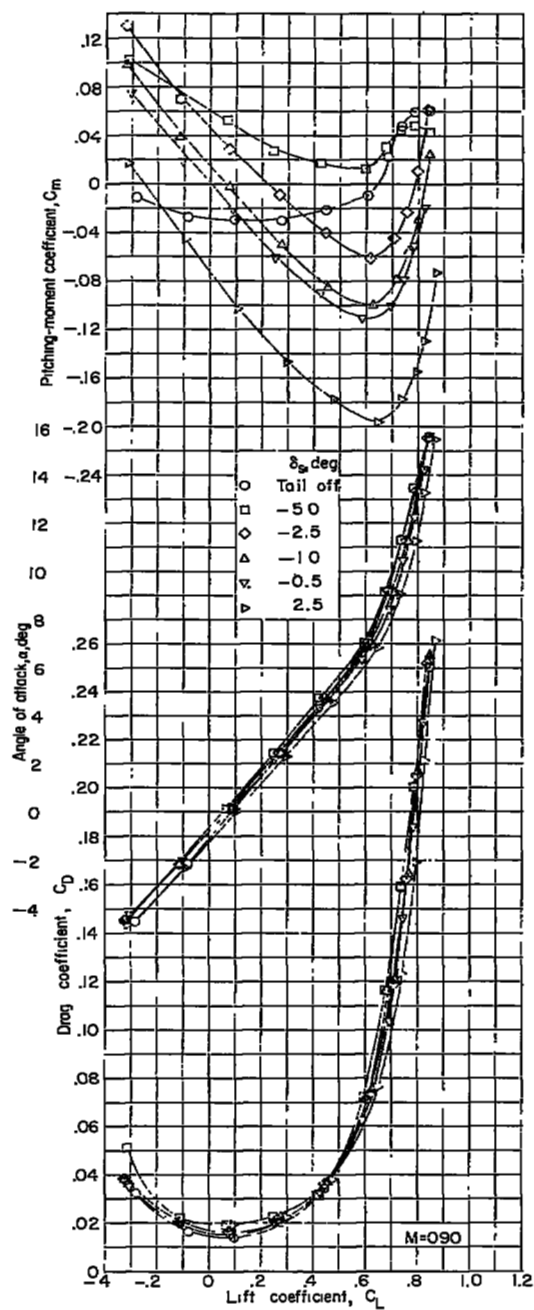
(b) $M = 0.90$ and 0.95 .

Figure 9.- Continued.

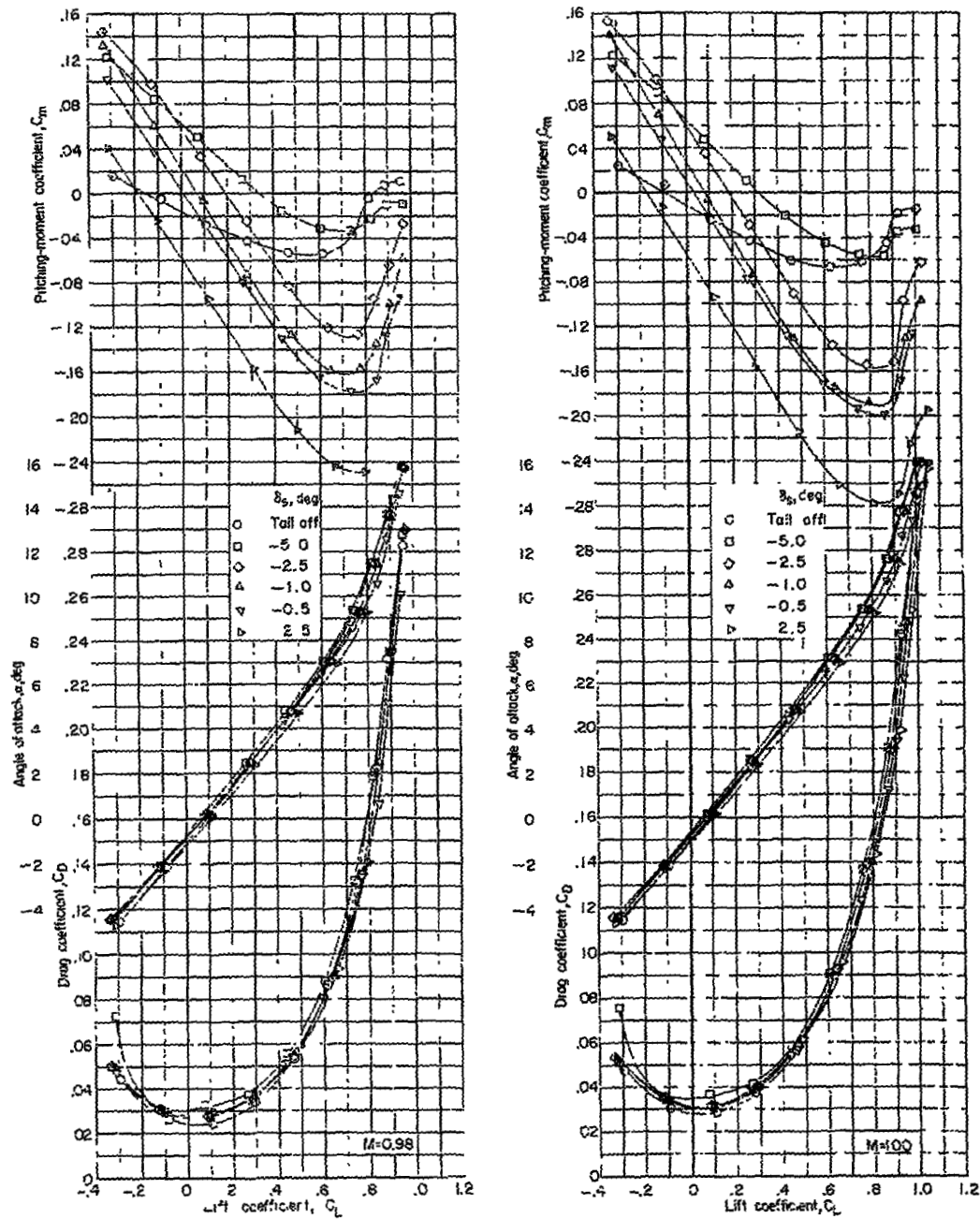
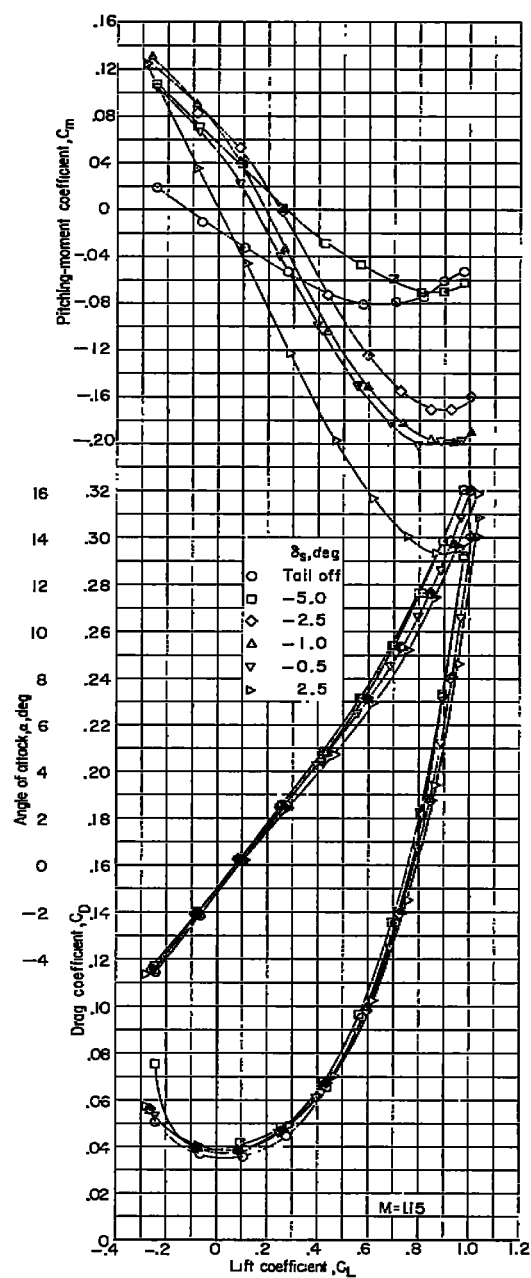
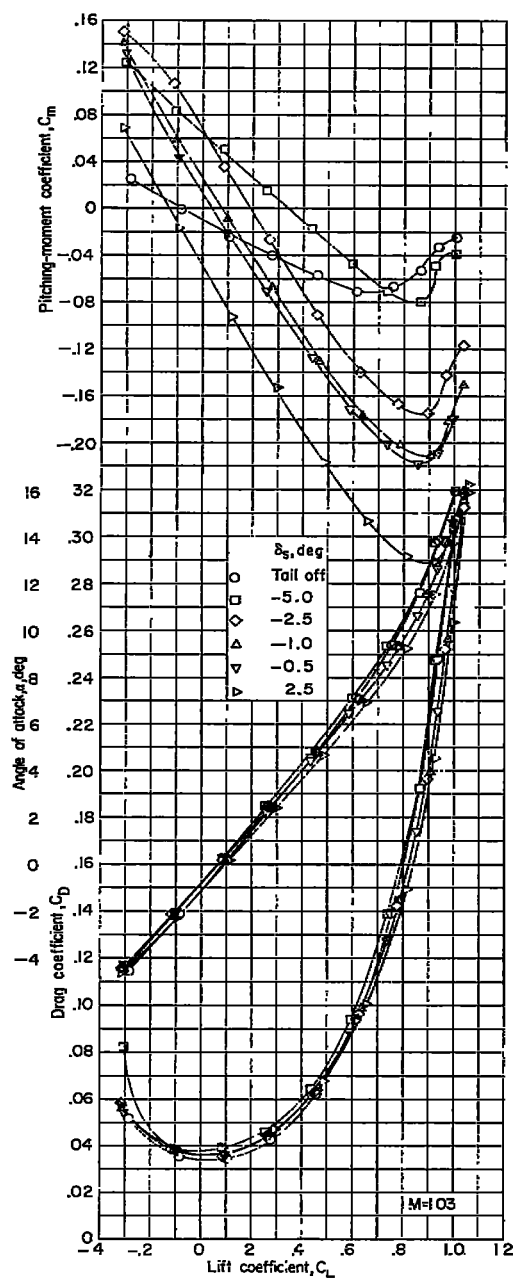
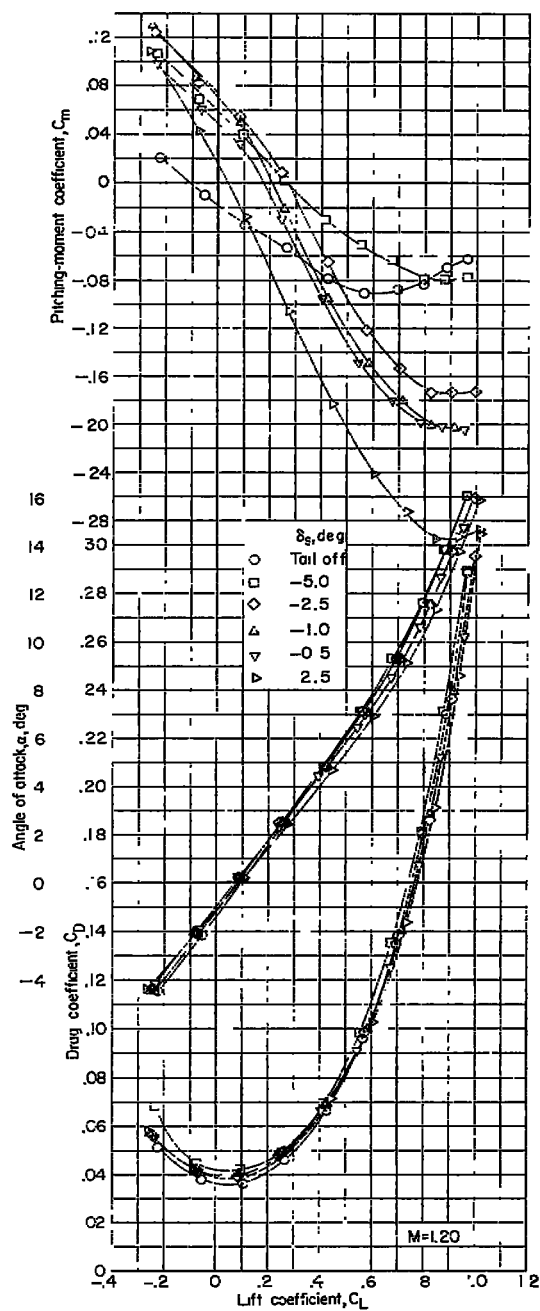
(c) $M = 0.98$ and 1.00 .

Figure 9.- Continued.



(d) $M = 1.03$ and 1.15 .

Figure 9.- Continued.



(e) $M = 1.20$.

Figure 9.- Concluded.

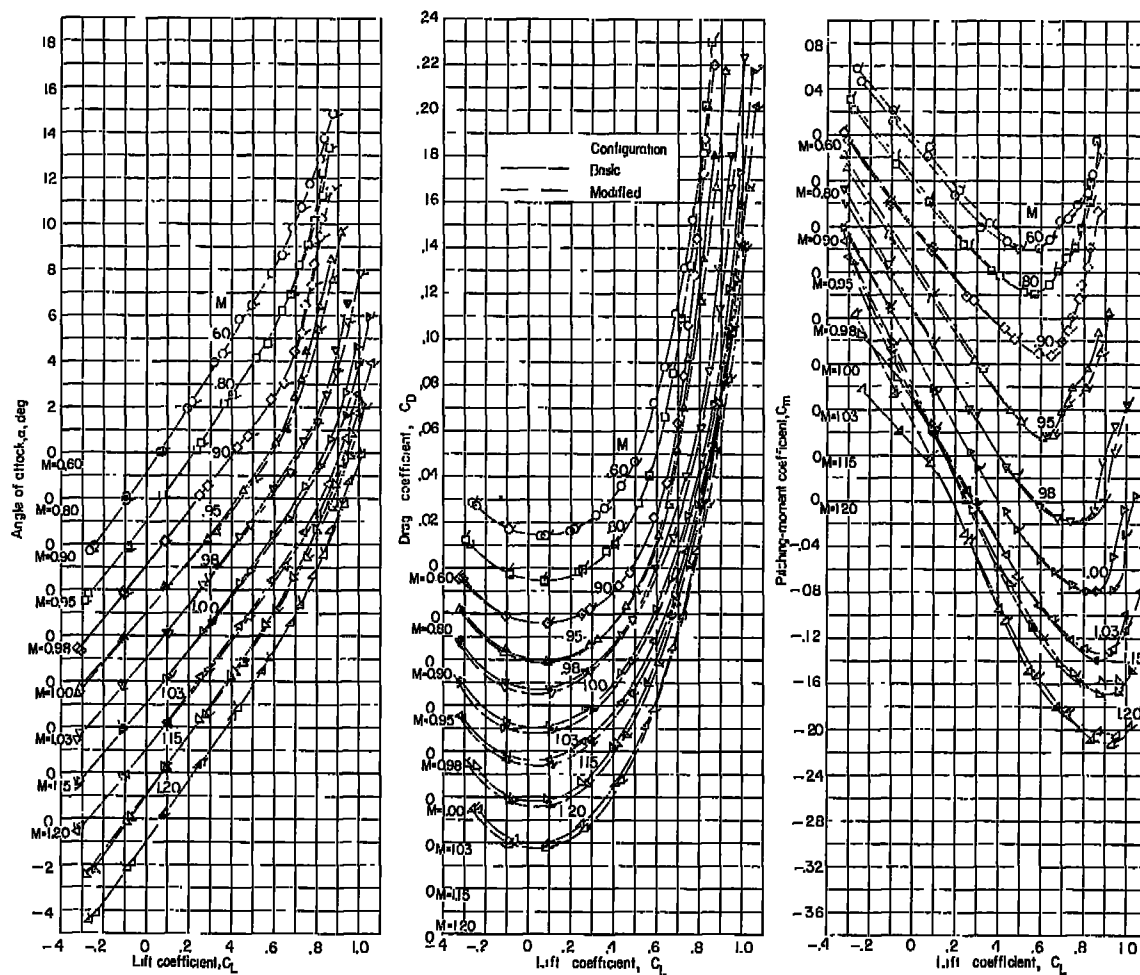


Figure 10.- Effect of hull modification on the aerodynamic characteristics of the model. Horizontal tail on; $\delta_s = -0.5^\circ$. (Plain symbols and solid lines indicate basic configuration; flagged symbols and broken lines indicate modified configuration.)

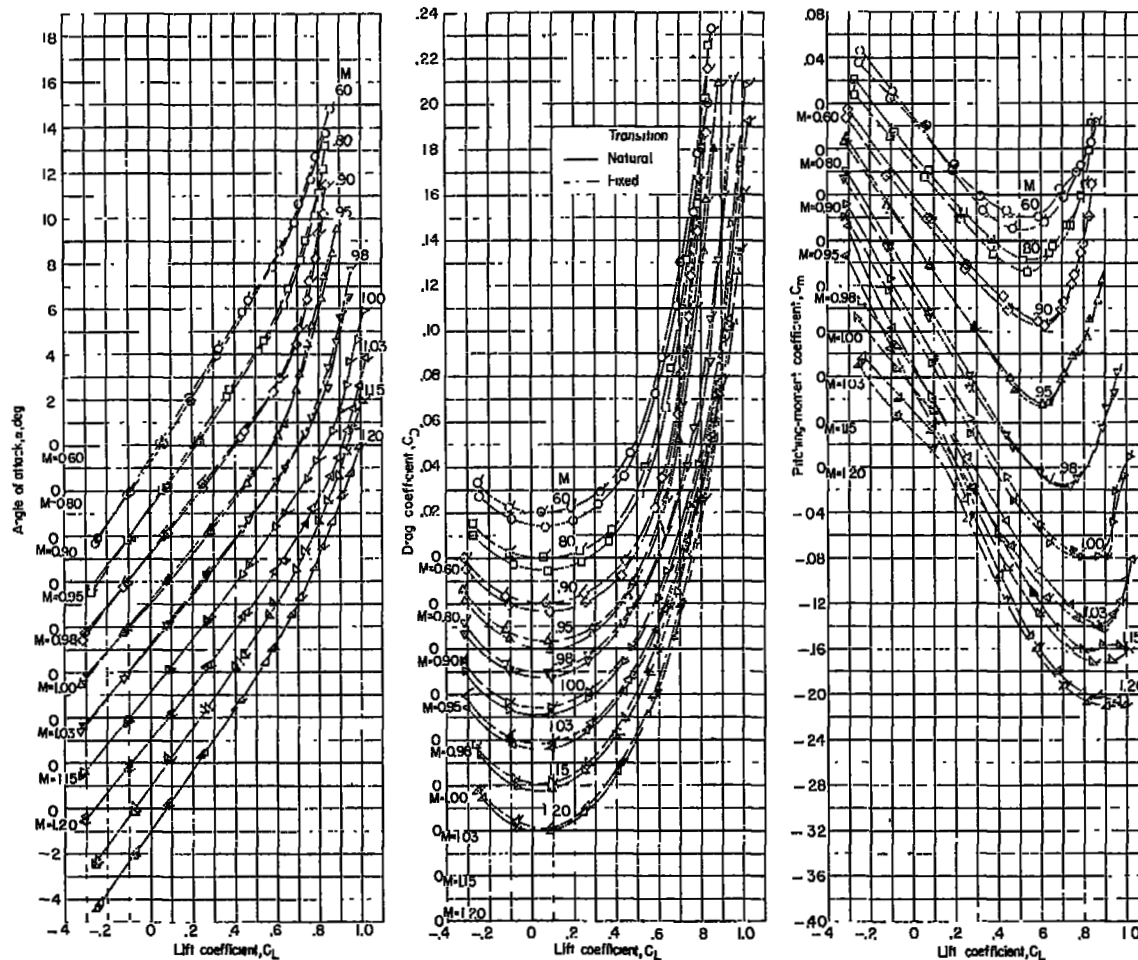


Figure 11.- Effects of fixed transition on the aerodynamic characteristics of the basic configuration. Horizontal tail on; $\delta_s = -0.5^\circ$. (Plain symbols and solid lines indicate natural transition; flagged symbols and broken lines indicate fixed transition.)

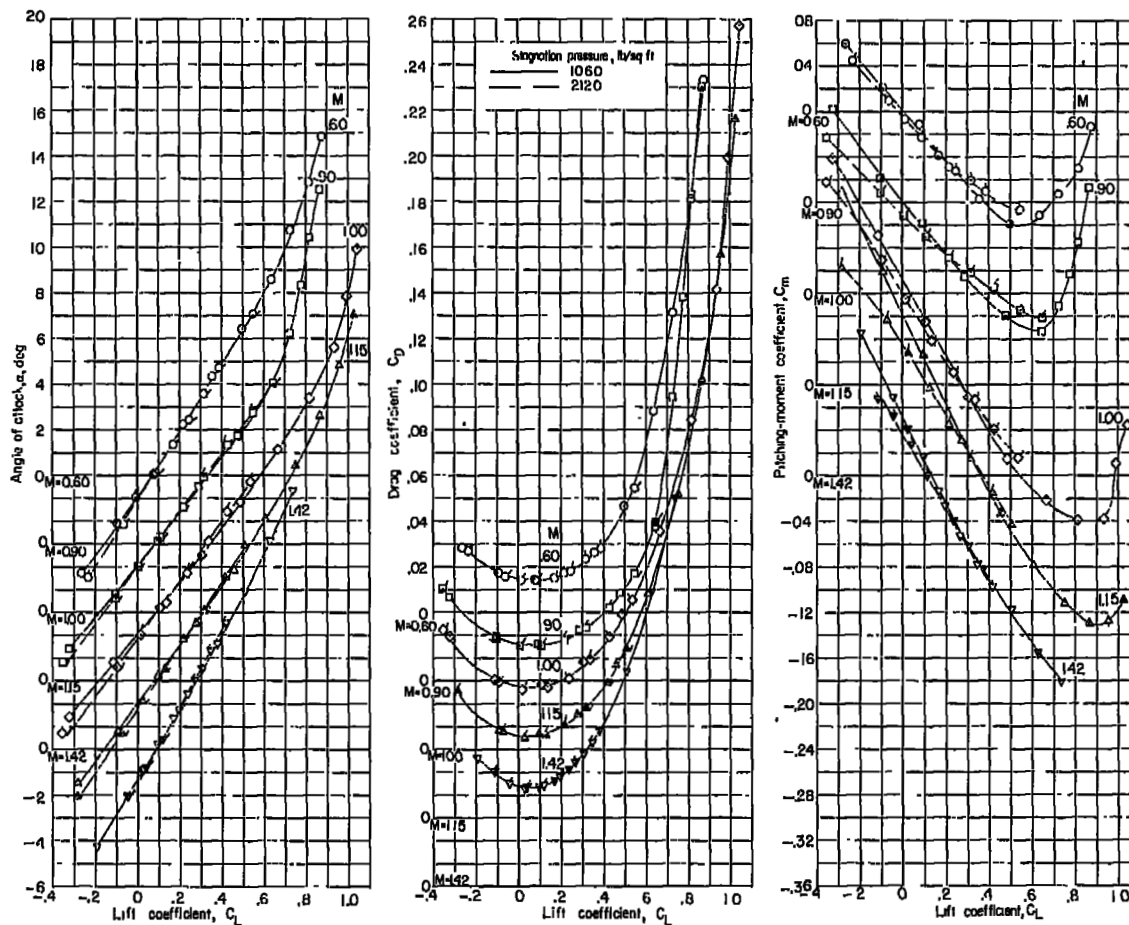


Figure 12.- Effect of stagnation pressure on the aerodynamic characteristics of the modified configuration. Horizontal tail on; $\delta_s = -0.5^\circ$. (Plain symbols and solid lines indicate stagnation pressure of 1,060 lb/sq ft; flagged symbols and broken lines indicate stagnation pressure of 2,120 lb/sq ft.)

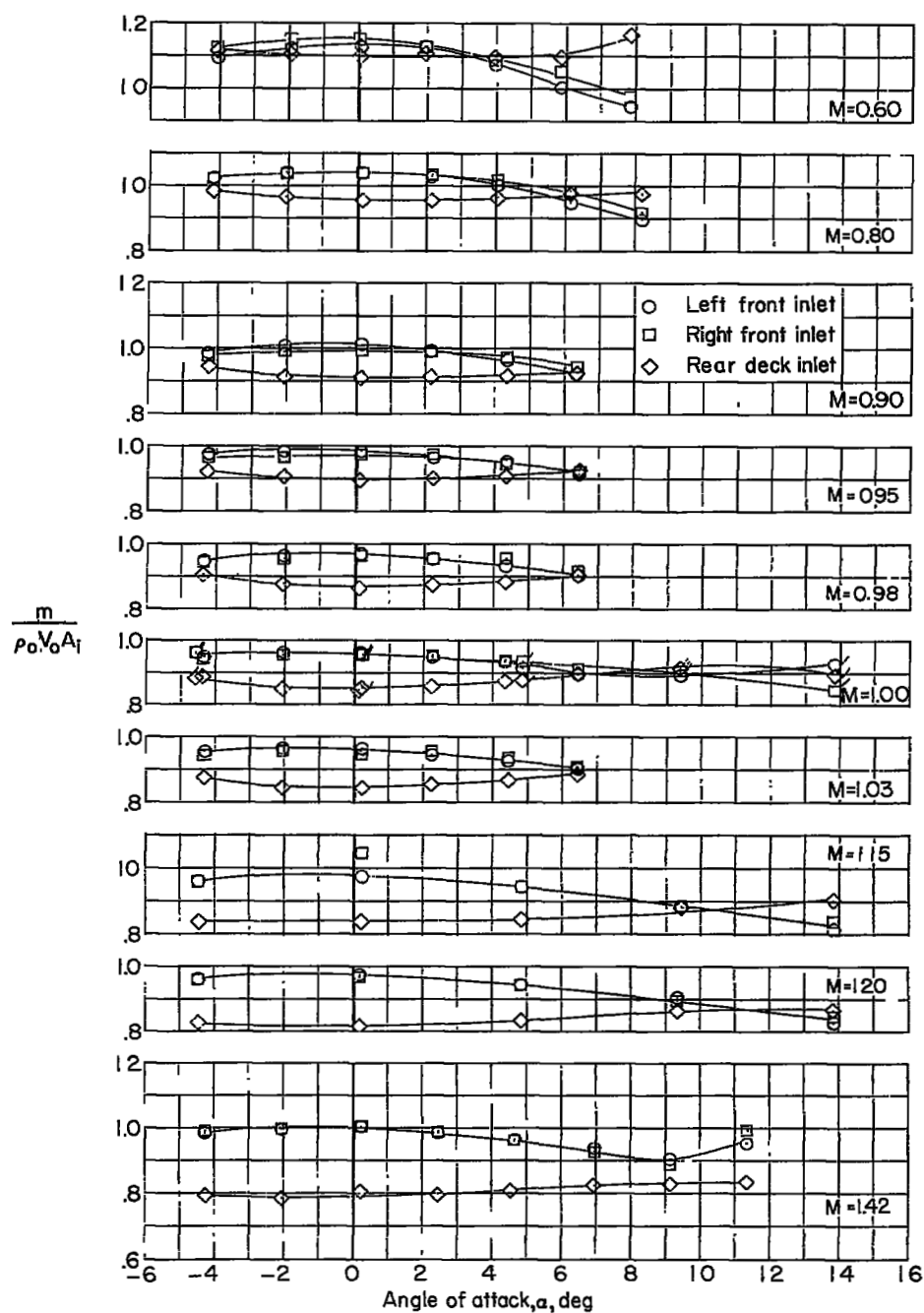


Figure 13.- Variation with angle of attack of the mass-flow ratio for the basic configuration. Flagged symbols indicate repeat data.

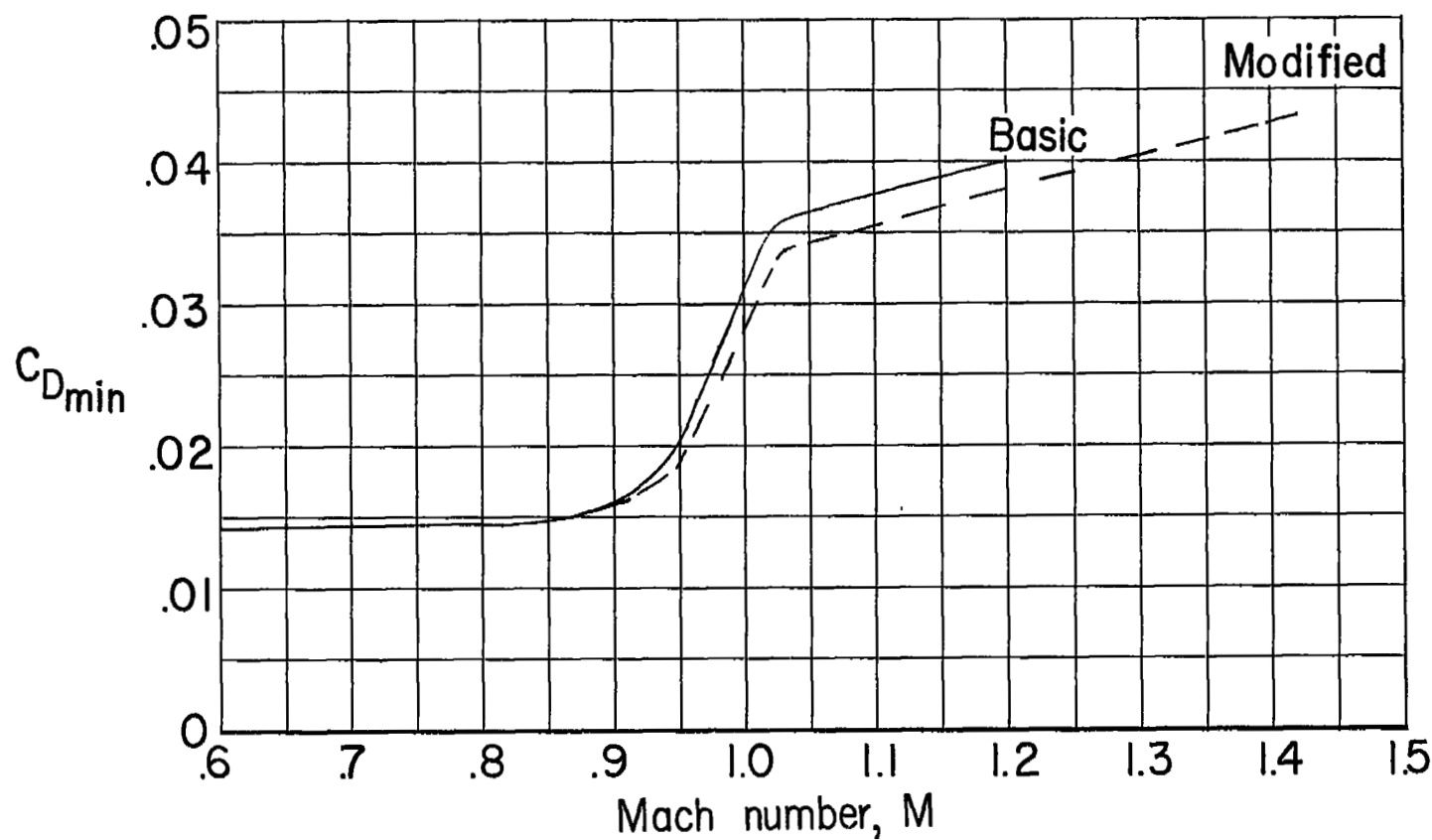


Figure 14.- A comparison of the minimum drag coefficients of the basic and modified configurations. $\delta_g = -0.5^\circ$.

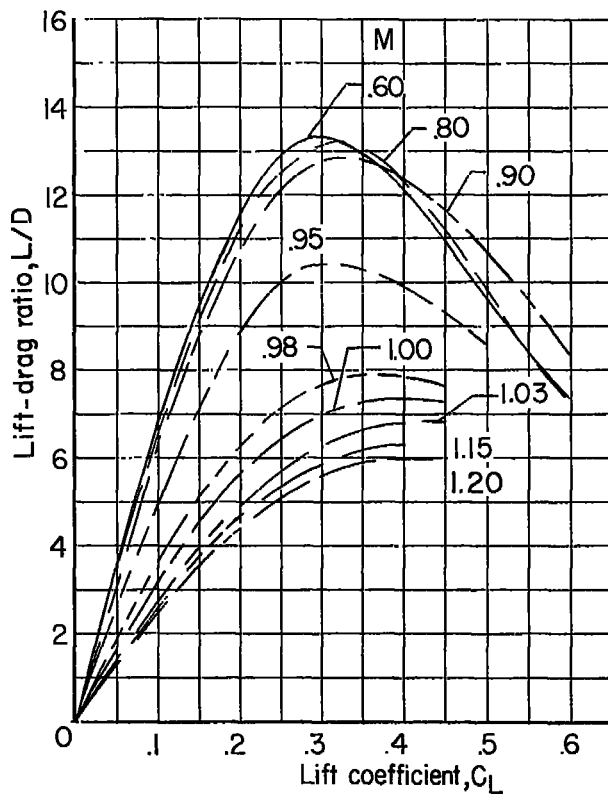


Figure 15.- Variation with lift coefficient of the trim lift-drag ratio at various Mach numbers for the basic configuration.

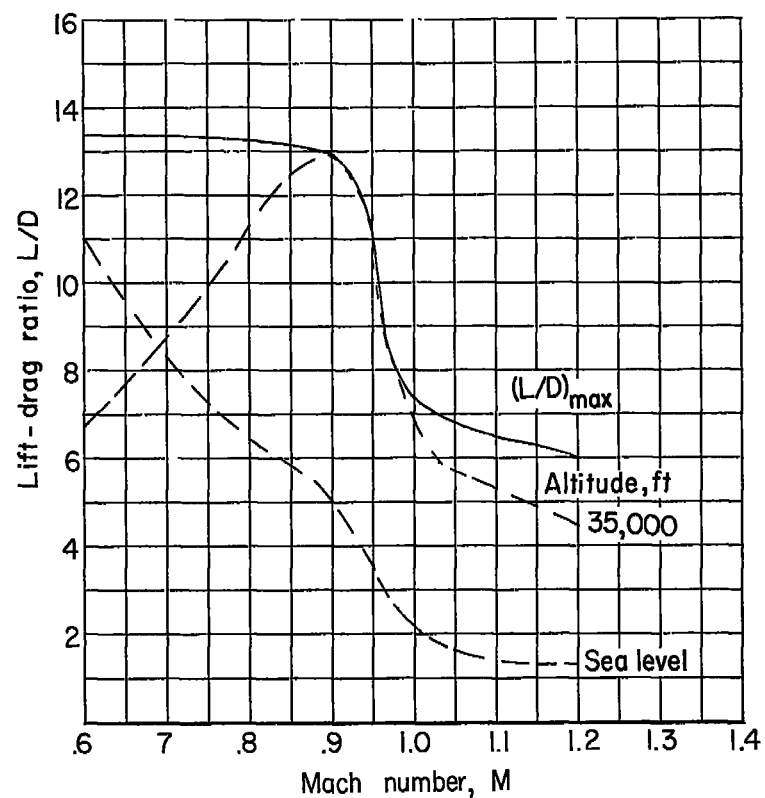


Figure 16.- Variation with Mach number of the maximum trim lift-drag ratio and of the trim lift-drag ratio in level flight for sea level and 35,000 feet altitude for a wing loading of 100 pounds per square foot.

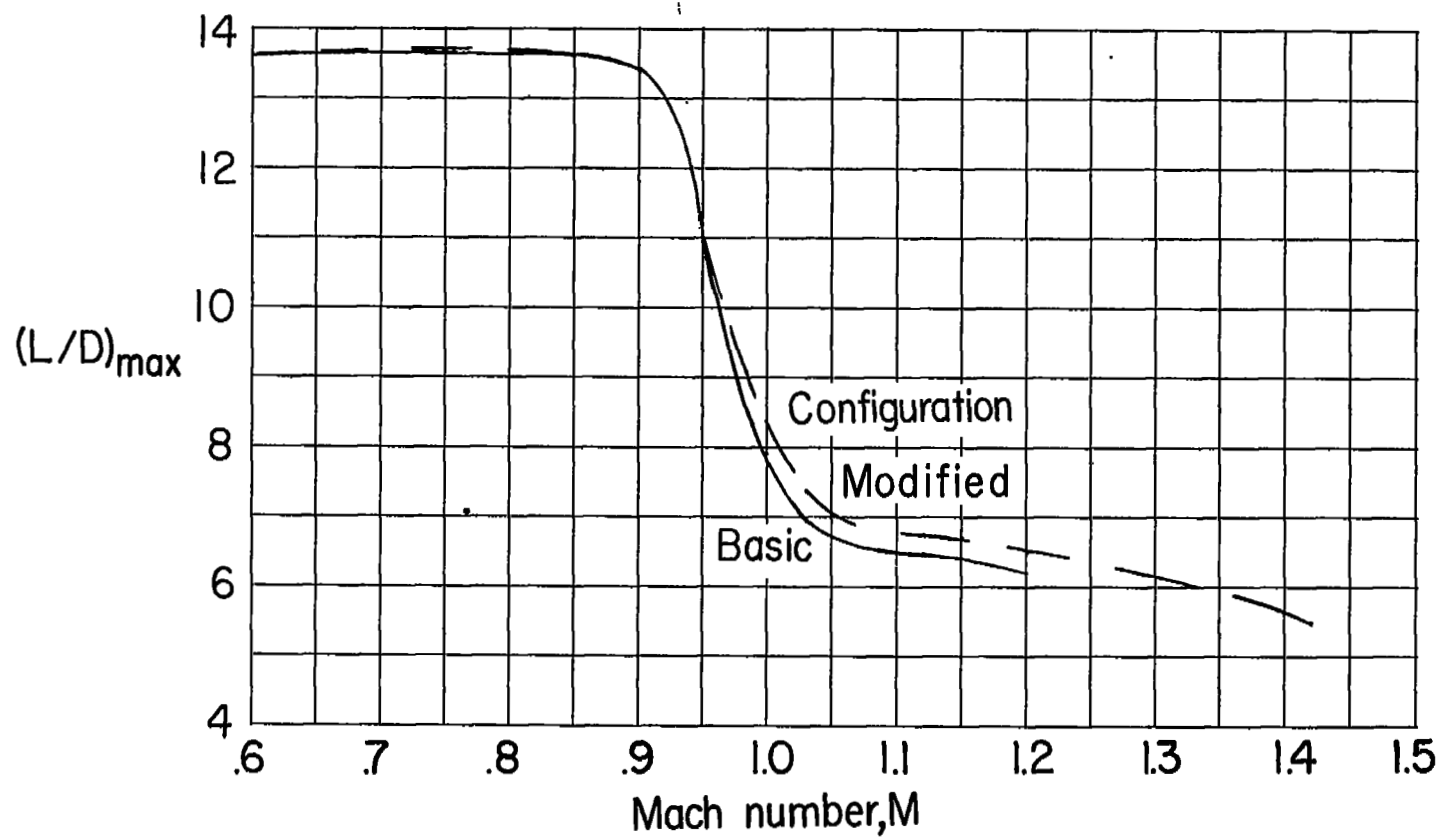


Figure 17.- Variation with Mach number of the maximum lift-drag ratios for the basic and modified configurations untrimmed.

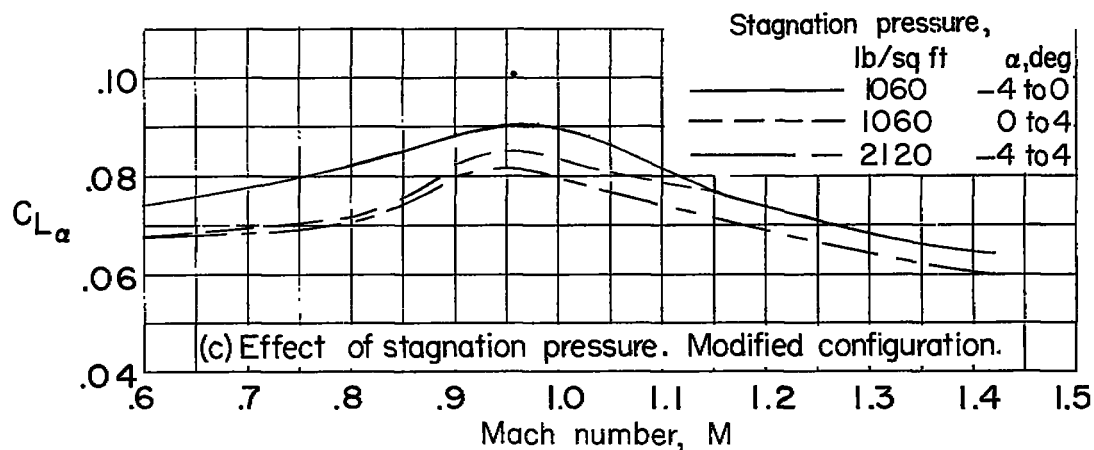
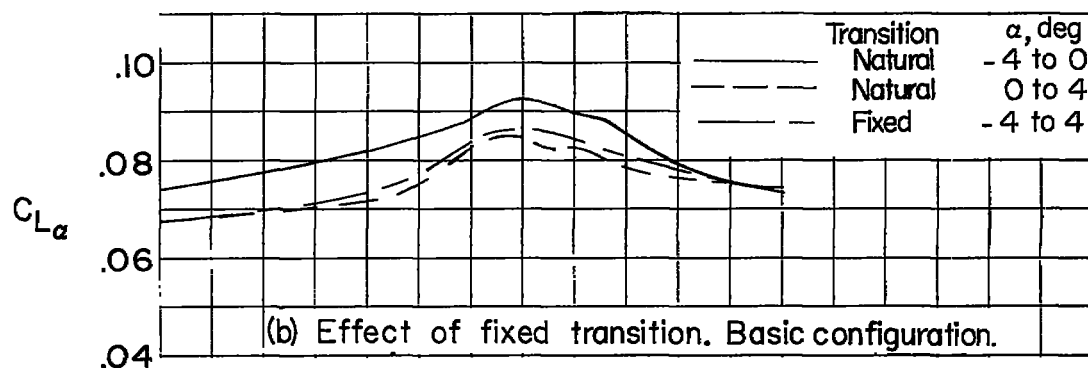
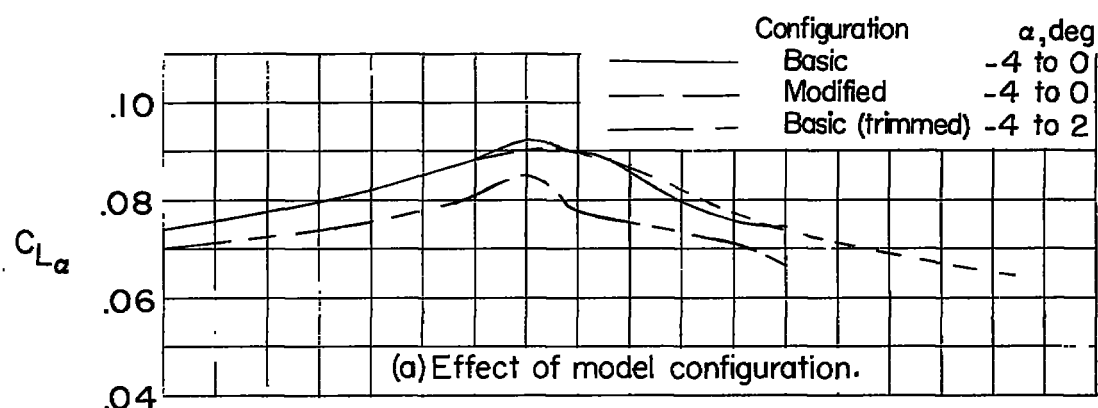


Figure 18.- Variation with Mach number of the lift-curve slopes for various model configurations.

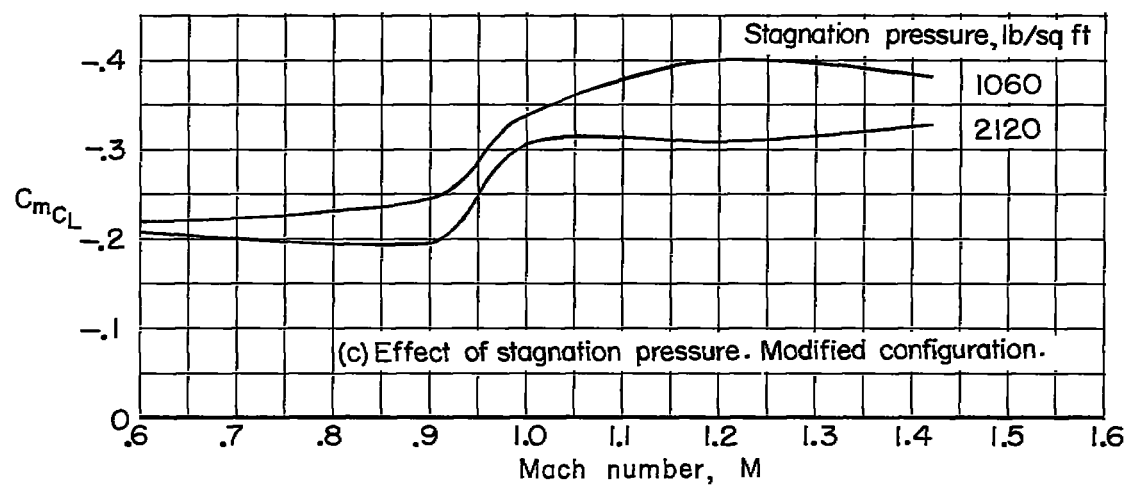
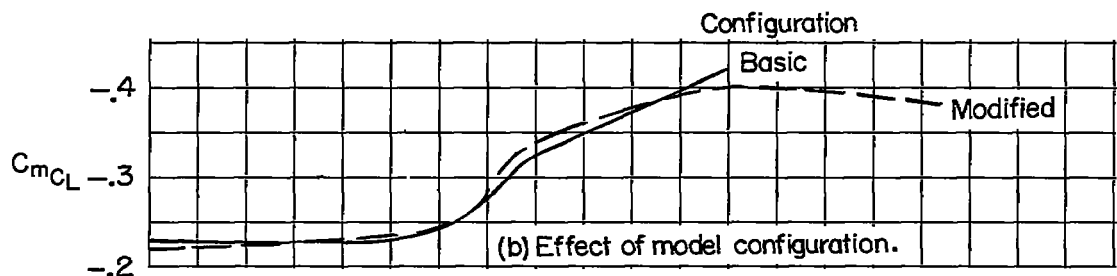
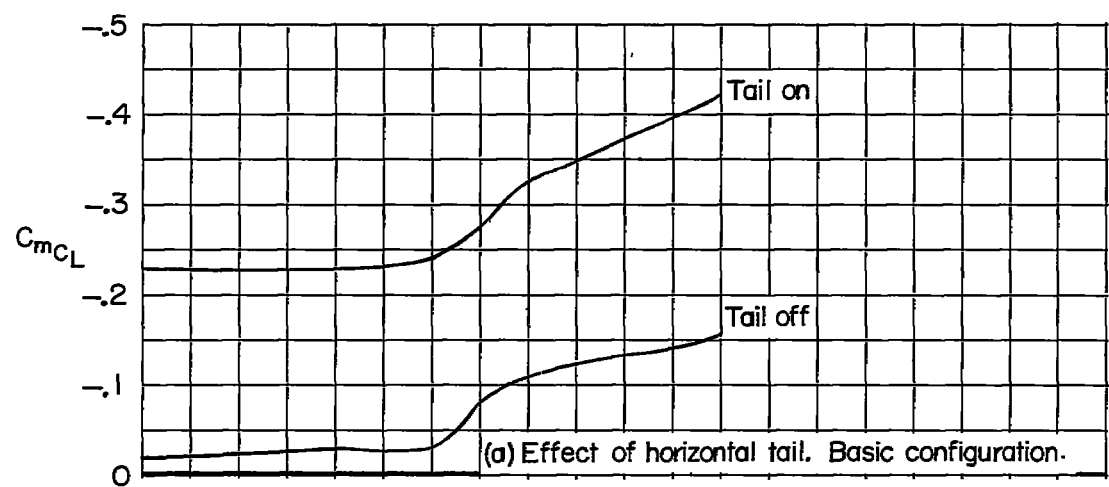


Figure 19.- Variation with Mach number of the pitching-moment-curve slopes for various model configurations.

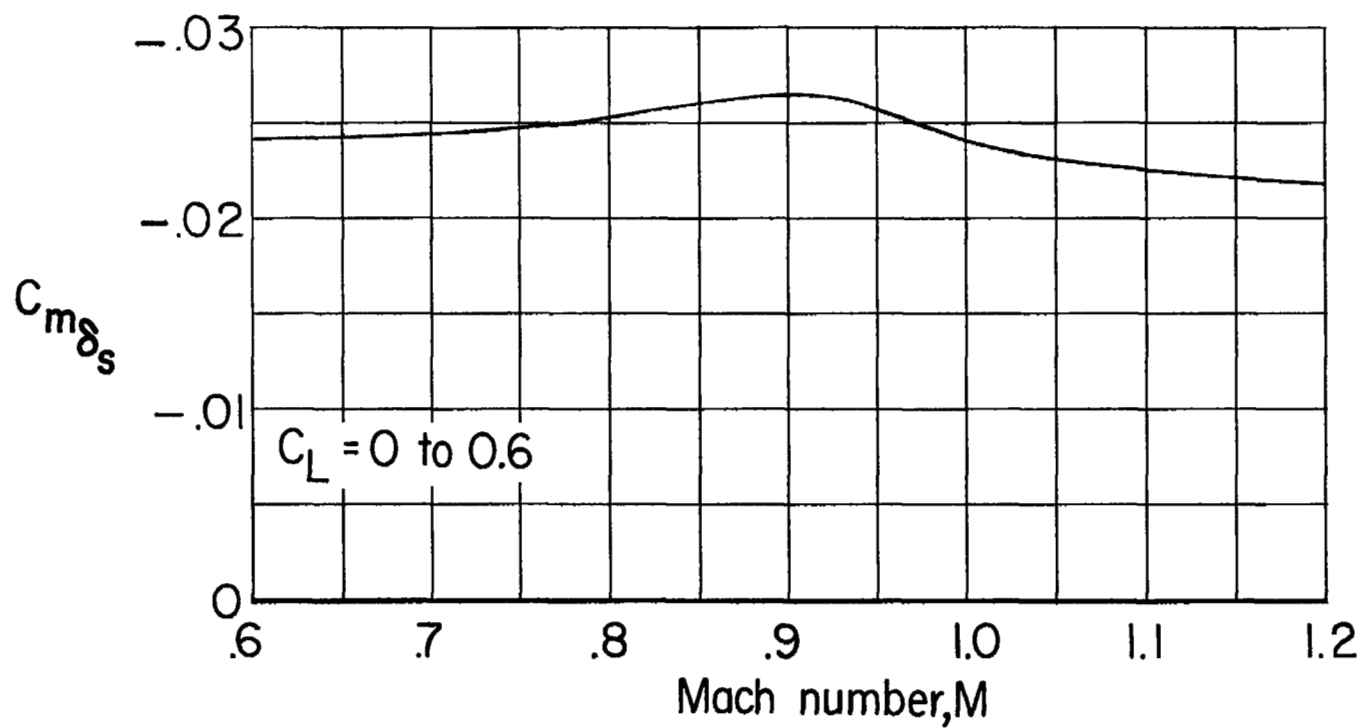


Figure 20.- Variation with Mach number of the stabilizer effectiveness parameter.

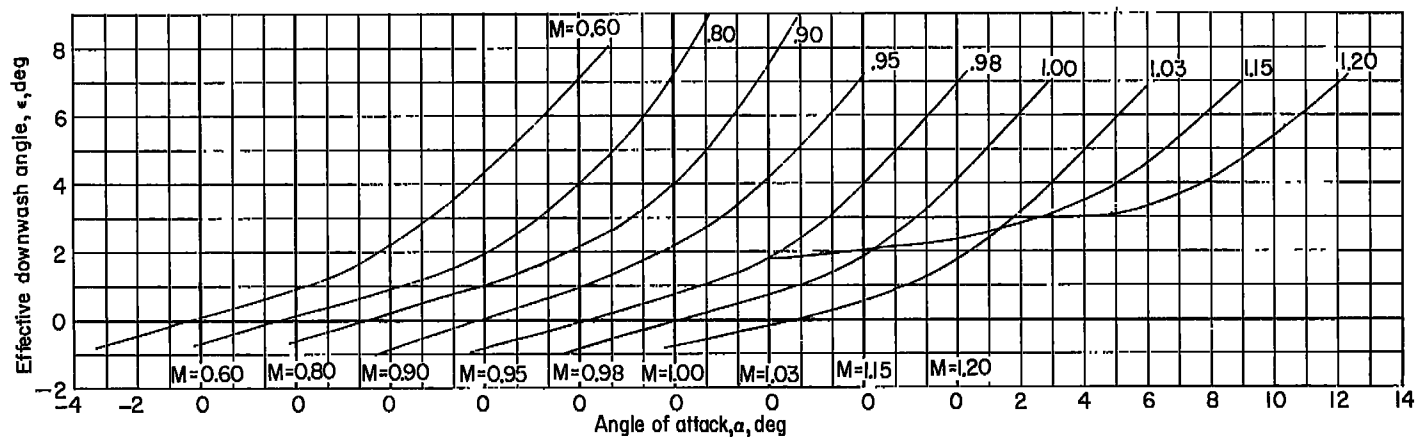


Figure 21.- Variation of the effective downwash angle with angle of attack for the basic configuration.

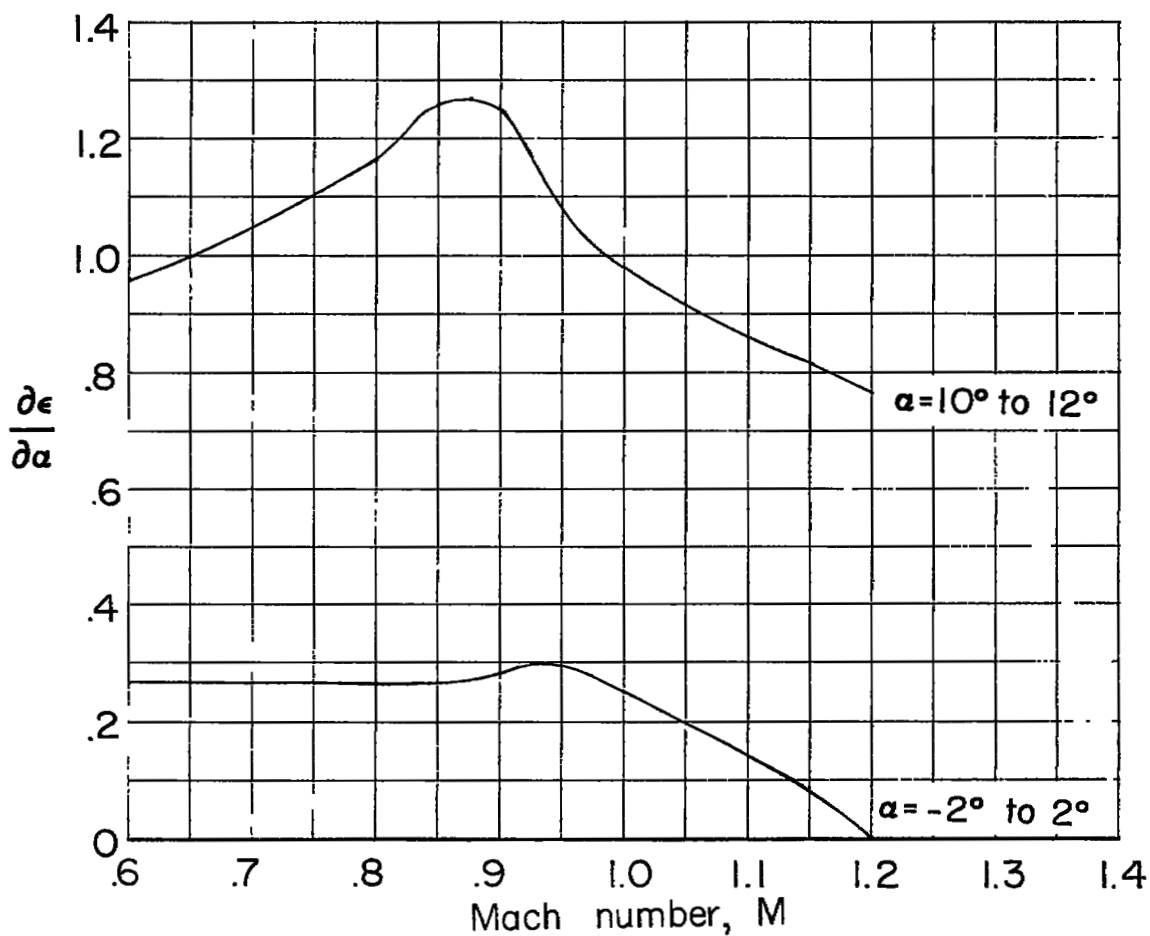
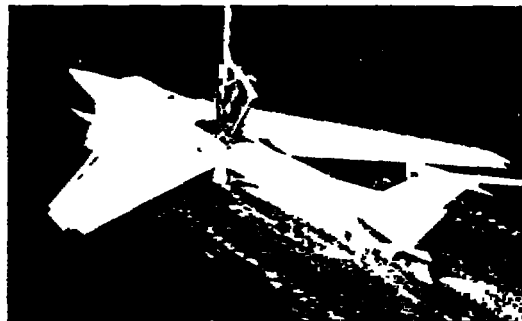
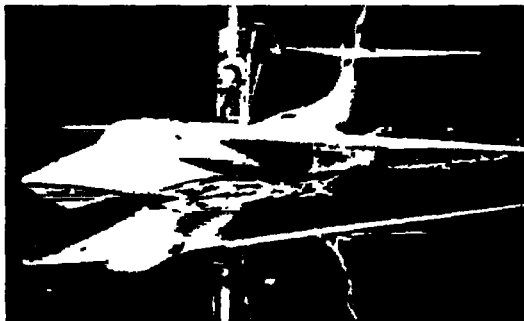
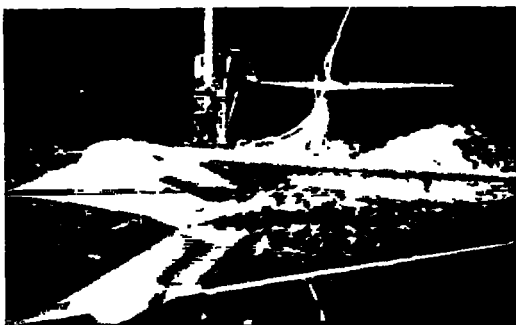


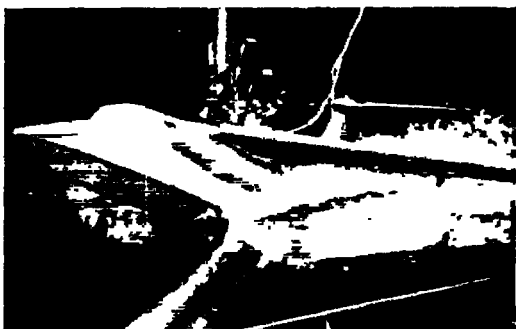
Figure 22.- Variation with Mach number of the rate of change of effective downwash angle with angle of attack for the basic configuration.



Speed, 24.9 knots; trim, 5° ; flap deflection, 0° .



Speed, 43.4 knots; trim, 6.2° ; flap deflection, 0° .



Speed, 61.8 knots; trim, 10.1° ; flap deflection, 0° .

Figure 23.- Typical spray photographs.

L-93583



Speed, 80.6 knots; trim, 10.3° ; flap deflection, 0° .



Speed, 84.4 knots; trim, 9.8° ; flap deflection, 40° .



Speed, 104.7 knots; trim, 8.9° ; flap deflection, 40° .

Figure 23.- Concluded.

L-93584

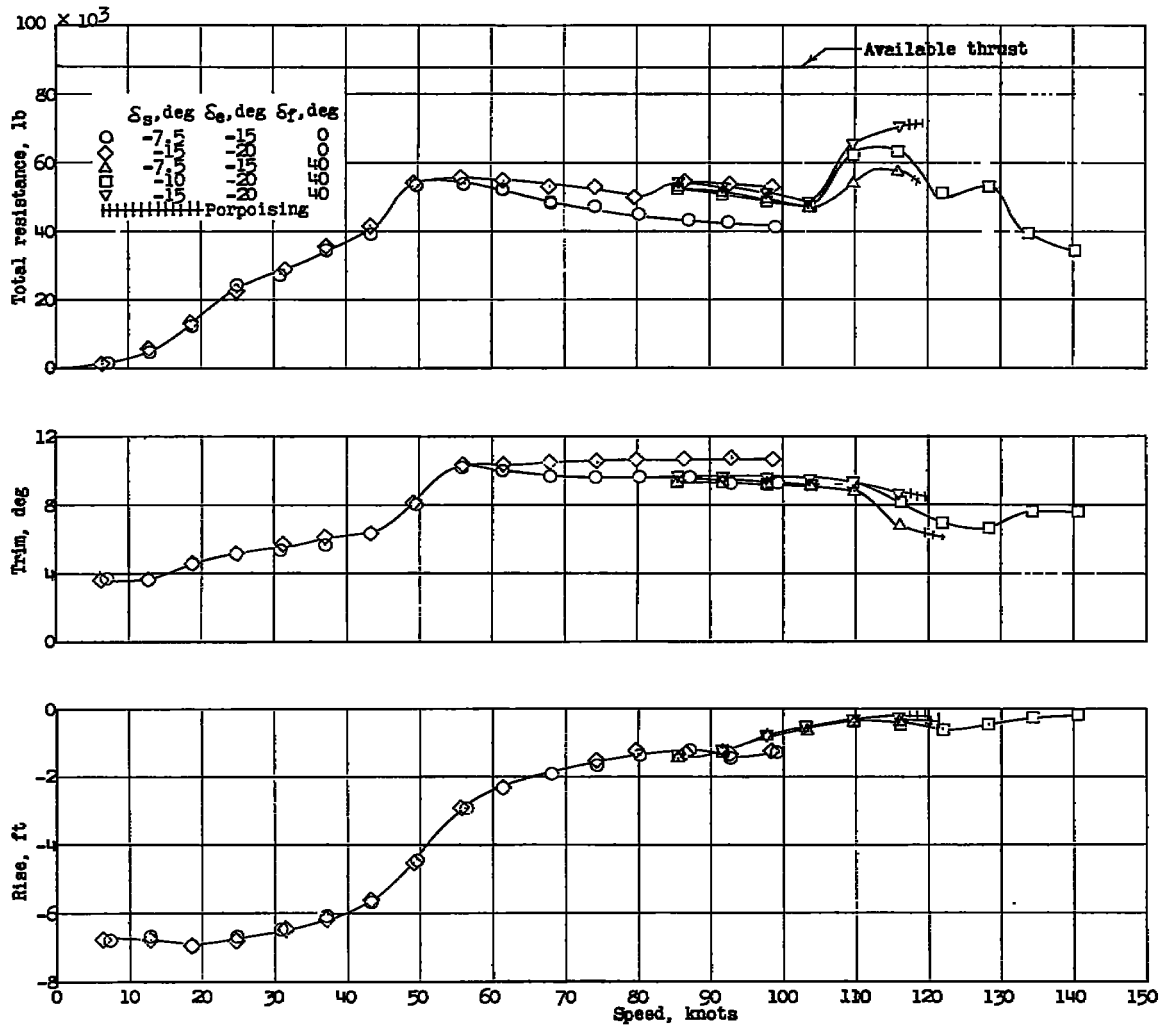


Figure 24.- Variation in total resistance, trim, and rise with speed.
 $\delta_f = 0^\circ$ and 40° .

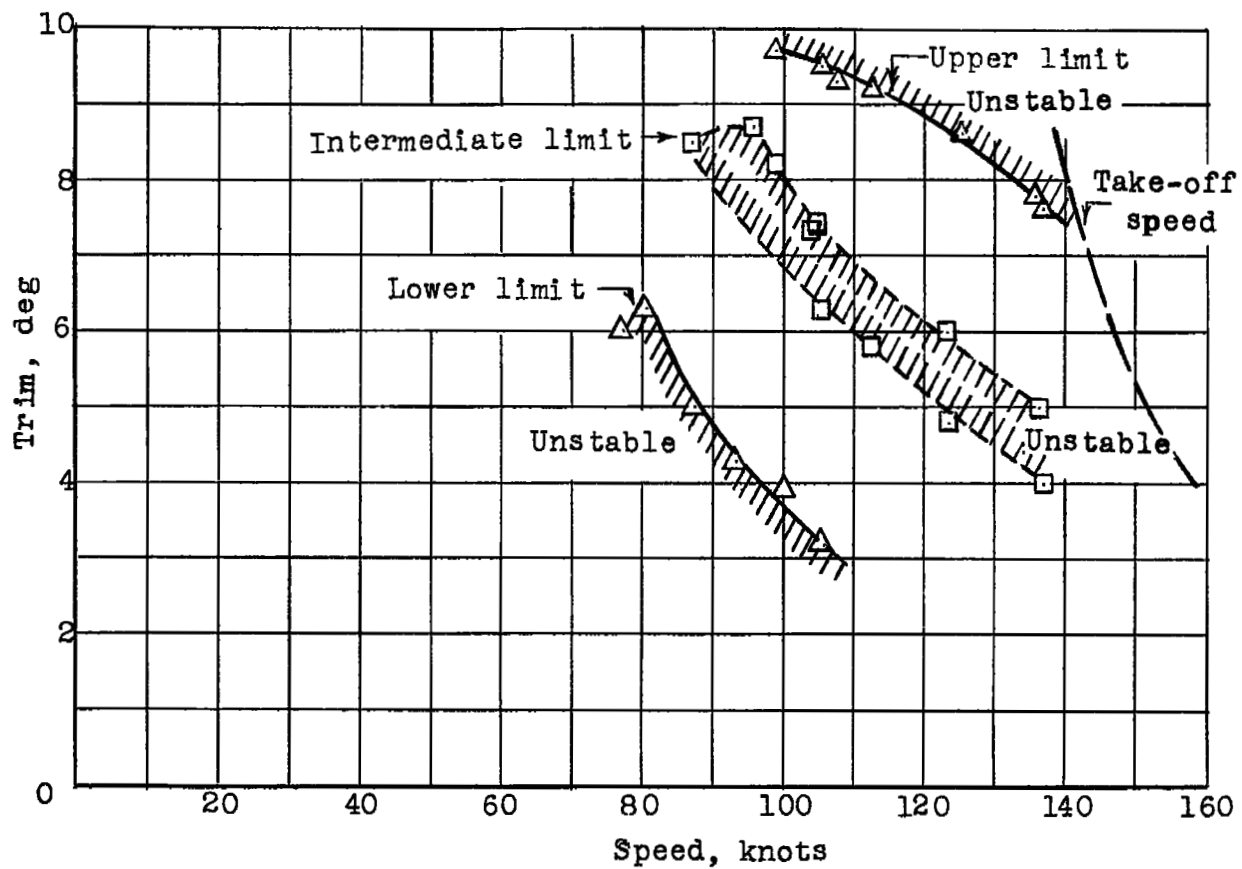


Figure 25.- Trim limits of stability. $\delta_F = 40^\circ$.

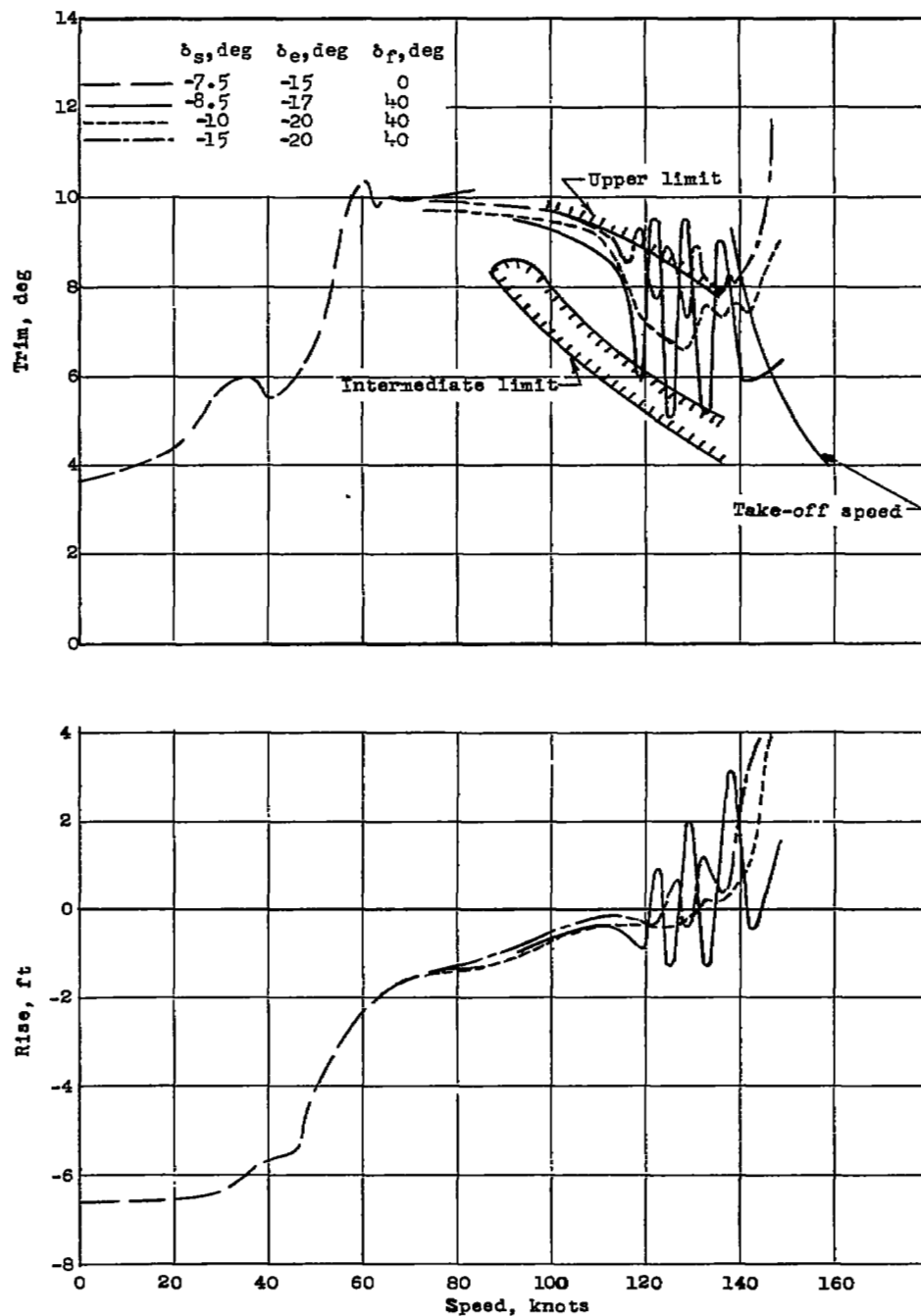
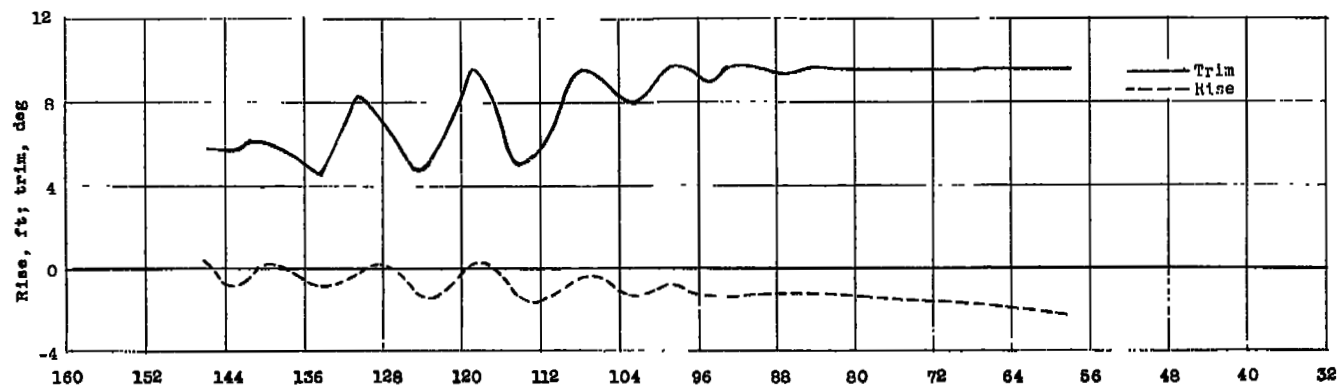
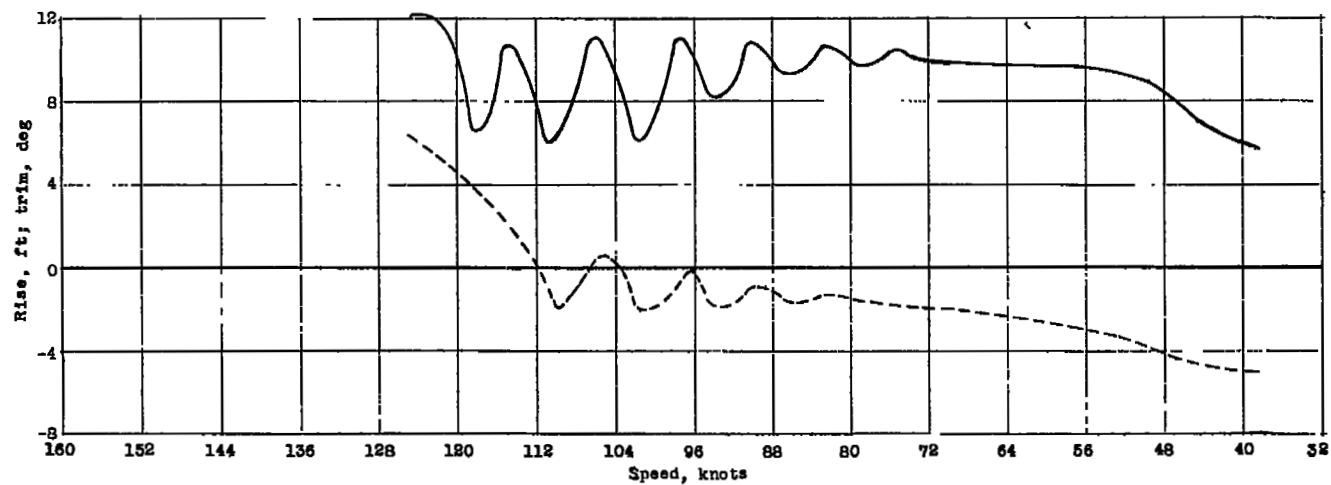


Figure 26.- Variation in trim and rise during smooth-water take-offs for various elevator deflections.

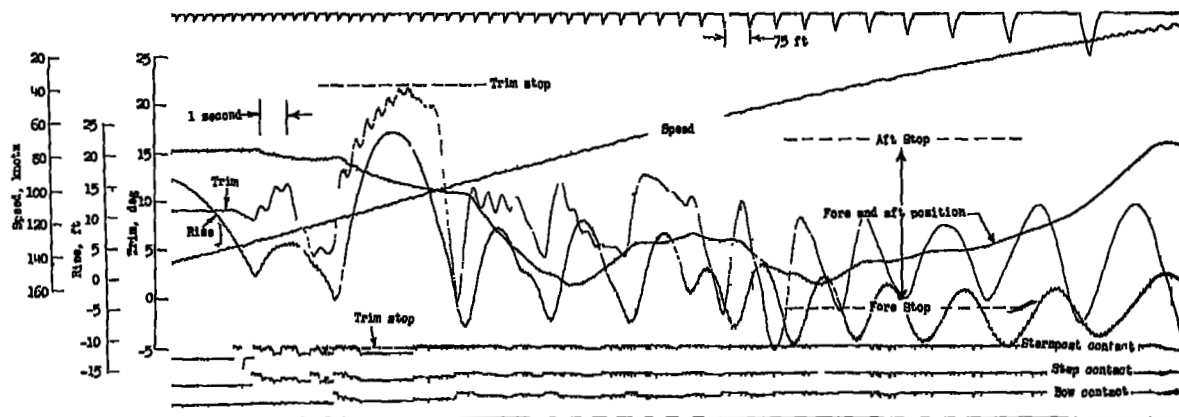


(a) Landing trim, 5.7° .

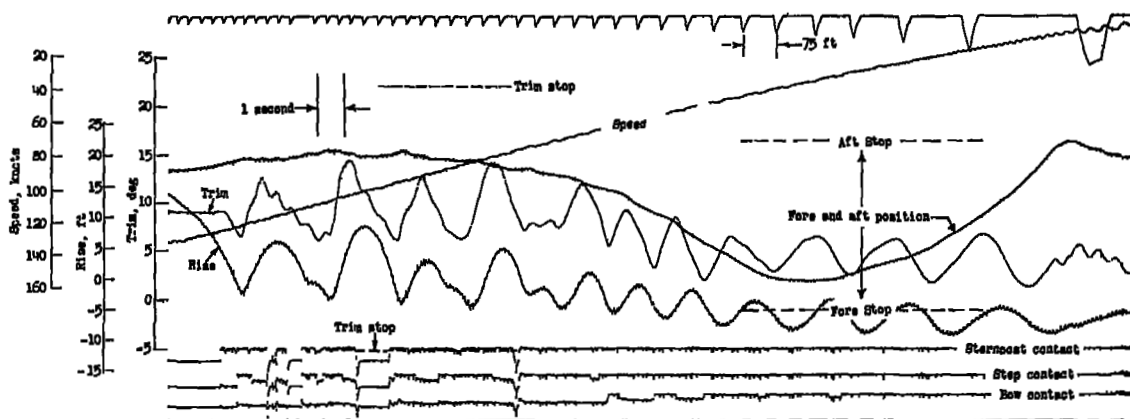


(b) Landing trim, 12.1° .

Figure 27.- Variation in trim and rise during typical smooth-water landings. $\delta_F = 40^\circ$.

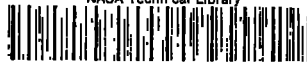


(b) Waves 8 feet high and 255 feet long.



(a) Waves 4 feet high and 255 feet long.

Figure 28.- Typical records of landings in waves.



3 1176 01437 7403



7
1

7
1

7
1

~~CONFIDENTIAL~~